GLOBAL MODEL FOR HIGH PRESSURE ELECTRONEGATIVE RADIO-FREQUENCY DISCHARGES

by

Y. T. Lee, M. A. Lieberman, A. J. Lichtenberg,
F. Bose, H. Baltes, and R. Patrick

Memorandum No. UCB/ERL M96/23

15 April 1996

GLOBAL MODEL FOR HIGH PRESSURE ELECTRONEGATIVE RADIO-FREQUENCY DISCHARGES

by

Y. T. Lee, M. A. Lieberman, A. J. Lichtenberg,
F. Bose, H. Baltes, and R. Patrick

Memorandum No. UCB/ERL M96/23

15 April 1996

ELECTRONICS RESEARCH LABORATORY

College of Engineering
University of California, Berkeley
94720

Abstract

We develop a global model for high pressure (0.1–1 Torr) electronegative radio frequency (RF) discharges and apply it to model capacitively driven plasma etchers. The molecular gases considered consist of either pure chlorine species or a mixture of chlorine and helium species. The charged and neutral heavy particle densities together with the electron density and electron temperature are calculated by using the equations of particle balance and power balance for the input discharge parameters RF power or RF current, inlet pressure, gas flowrates, reactor diameter, and gap spacing. The power is deposited in the electrons via ohmic heating and in those ions accelerated across the DC sheath potential. The voltage across the sheath is calculated self consistently with the densities and the electron temperature by using a collisional Child law sheath model. Analytic scaling laws for the dependence of charged and neutral particle densities, electron temperature, RF voltage and current, sheath width, and plasma impedance on pressure and absorbed RF power are presented and used to explain the numerical results obtained from the global model. The model results are compared to recent experimental measurements in a chlorine discharge over a range of absorbed power $P_{abs} = 20 - 180$ W at an inlet pressure $p_{in} = 0.4$ Torr and a range of pressure 0.1–1.6 Torr with fixed input power of 100 W. We obtain reasonable agreement for $P_{abs} < 200$ W and for 0.2 Torr $< P_{in} < 1$ Torr.

1 Introduction

High pressure electronegative discharges are used in the microelectronics industry for etching of sub-micron integrated- circuit devices and liquid crystal flat panel displays. For example, the chlorine/helium discharge in a Lam 490 etcher is typically operated at an inlet pressure of few hundred mTorr and a radio frequency (RF) power of several hundred watts[1]. The discharge consists of two parallel plates with a radius of 10.16 cm and a separation of 2.0 cm. In processing microelectronics devices, the input parameters such as pressure, RF power, and gas flows are varied to achieve optimal etch rate and etch uniformity.

Recently, global models have been developed for different molecular gases and successfully applied to model high density, low pressure discharges such as RF driven transformer-coupled-plasma sources[2,3]. We develop a global model for a high-pressure electronegative RF discharge and apply it to model capacitively driven plasma etchers. In this model, the densities of the neutral species are uniform throughout the discharge. We also assume that the electron density is uniform throughout the plasma except at the sheath region near the edge of a discharge. For each neutral or charged species, we construct a particle balance equation that includes volume generation and destruction and diffusion loss to the wall. Neutral species also flow into and out of the discharge as a result of pumping. For the charged species, we use the approximation that the positive and negative ion densities have parabolic profiles and we assume a uniform density for the electrons[4-6] except at the sheath interface. The scale length of the profile is in principle determined by the Bohm condition applied at the edge of the plasma, but in a high

pressure discharge with high electronegativity, the scale length of the profile is approximately equal to the plasma length[6]. The ambipolar diffusion coefficient of the positive ions is taken to be constant throughout the plasma, which includes the presence of both electrons and negative ions. The flux of positive ion loss to the wall is then calculated by using the ambipolar diffusion coefficient and the parabolic profile. Negative ion loss to the wall is neglected since these ions are strongly confined by the ambipolar potential. The gas and ion temperatures are assumed to be constant independent of the discharge condition. The electron temperature is assumed to be uniform throughout the plasma and its value is determined by the particle balance of charged species in the discharge. These assumptions constitute our global model.

To obtain a complete model we introduce the heating mechanisms and sheath characteristics as follows. The RF power is deposited in the electrons via ohmic heating (with sheath heating neglected at the high pressures considered) and in those ions accelerated across the DC sheath potential. The power deposited in the electrons balances the energy losses due to the processes of electron-neutral collisions such as elastic scattering, rotational, vibrational, and electronic excitation, ionization, dissociation, dissociative attachment, and electron detachment. The DC voltage across sheath is calculated self consistently with the densities and electron temperature by using a collisional Child law sheath model[7]. The complete set of particle continuity and power balance equations are solved self consistently to obtain the densities for all the species and the electron temperature.

In the next section, we describe the formulation of the global model for capacitively driven discharges. The set of particle continuity and power bal-

ance equations is given. In Section 3, we apply the global model to mixed chlorine/helium feedstock gases and to chlorine feedstock gas with discharge dimensions corresponding to the Lam 490[1] etchers. The densities of all the species together with the electron temperature are calculated for a range of inlet pressures of 200–600 mTorr and absorbed RF power densities of 0.01–0.3 Wcm^{-2} or RF current densities of 0.001–0.1 amp-cm^{-2}. In Section 4, we derive analytic scaling laws for the dependence of the densities, electron temperature, total absorbed power, current, and voltage on inlet pressure and RF power deposited in electrons and show that the scalings are consistent with the more general numerical results of Sec. 3. In Section 5, we compare the model results to recent experimental measurements performed with Lam 490 plasma etcher. Our results agree reasonably well with the experimental measurements. We present the conclusion of our paper in Section 6.

2 Global Model Formulation

2.1 Neutral particle balance

We consider a one-dimensional cylindrical discharge geometry with its radius R much greater than its height l_s. A schematic drawing for the cross section of the discharge is shown in Fig. 1. At high electronegativity, the positive and negative ions have approximately the same parabolic densities. Since the edge region of the electropositive plasma and the sheath is small compared to the bulk, we can approximate the plasma length to be l_s the gap spacing of the discharge and the scale length of the parabolic profile to be $l_s/2$. The electron density is taken to be uniform and is sufficiently small that it is not shown on the figure. The particle loss to the side of the cylinder is neglected

since it is small compared to the particle loss to the ends. The density of each neutral species is determined by the balance between the flowrate into the system, or the rate of dissociation of molecular into atomic species, and the residence time at a given partial pressure. For example, for the two neutral species of most interest, Cl_2 and Cl, the equations determining the density are

$$\frac{p_{in}}{kT_0\tau}\frac{q_{Cl_2}}{q_{tot}} + G_{Cl_2} = L_{Cl_2} + \frac{n_{Cl_2}}{\tau}, \tag{1}$$

$$G_{Cl} = L_{Cl} + \frac{n_{Cl}}{\tau}, \tag{2}$$

where p_{in} is the total inlet pressure (pressure of the gas in the absence of any plasma), T_0 is the neutral temperature in kelvins, k is Boltzmann constant, τ is the residence time, G and L are the volume generation and destruction rates, q_{Cl_2} is the flowrate of chlorine gas, and q_{tot} is the total flowrate of neutral species into the discharge. The residence time depends on the pressure of the discharge that is calculated based on all neutrals as $p = \sum n_j k T_0$, where n_j is the density of the j-th neutral species.

For chlorine atoms which can undergo surface recombination, we estimate the loss flux due to this process in terms of an equivalent volume loss rate as D_{eff}/Λ^2, where D_{eff} and Λ are the effective diffusion coefficient and length, respectively. Both D_{eff} and Λ are calculated as in Refs. 2 and 3.

2.2 Charged particle balance

The continuity equation for a charged species is written as

$$\frac{d}{dx}\Gamma_i = G_i - L_i, \tag{3}$$

where Γ_i is the flux. Integrating Eq.(3) and using the boundary condition that the flux is zero at the center of the discharge, we obtain the global

particle balance

$$\Gamma_i(l/2) = \int_0^{l/2} (G_i - L_i) dx, \tag{4}$$

where l is the plasma length. For negative ions the sheath voltage repels the ions such that $\Gamma_-(l/2) = 0$.

In general, in order to solve these equations it is necessary to obtain the spatial dependence of G_i and L_i by means of coupled diffusion equations, by substituting for the flux in Eq.(3) the relation

$$\Gamma_i = -D_i \frac{dn_i}{dx} \pm \mu_i n_i E, \tag{5}$$

where D_i is the diffusion coefficient and μ_i is the mobility. All the species are coupled through the electric field E. In a global model we make the assumption that the profiles $n_i(x)/n_{0,i}$ are known, where n_i is the positive or negative ion density and $n_{0,i}$ is the value of the density at the center of the discharge. In addition, we argue that a reasonable assumption is to use a parabolic profile for both the positive and negative ions[4-6] with a scale length of $l/2$

$$n_i(x) = n_{0,i} \left(1 - \frac{x^2}{(l/2)^2} \right). \tag{6}$$

Since we are concerned with highly electronegative plasmas, we can approximate the ambipolar diffusion coefficients of positive ion species as[4-5]

$$D_{i,a+} = 2D_{i,+}, \tag{7}$$

where the factor of two is a consequence of the weak electric field necessary to confine the negative ions and $D_{i,+} = \frac{T_i}{M_i \nu_{m,i}}$ with M_i the positive ion mass, T_i the ion temperature in eV, and $\nu_{m,i}$ the total ion-neutral momentum-transfer collision frequency. With this approximation, we have

$$\Gamma_{i,+} = -2D_{i,+} \frac{dn_i(x)}{dx}. \tag{8}$$

Substituting Eq.(6) in Eq.(8) and taking the derivative, we obtain the flux for positive ion loss to the wall as

$$\Gamma_{i,+} = \frac{4D_{i,+}n_{0,i}}{l/2}. \tag{9}$$

Since we are considering strongly electronegative plasmas with both negative species assumed to be in Boltzmann equilibrium, the internal electric fields are determined mainly by the cold negative ions and are small. Hence, $D_{i,a+} = 2D_{i,+}$ is much smaller than the ambipolar diffusion coefficient in the absence of negative ions,[4,5] $D_{i,a+} = D_{i,+}(1 + T_e/T_i)$, where T_e is the electron temperature. As a further consequence, the electrons are nearly uniform within the plasma,

$$n_e(x) \approx n_{0,e}. \tag{10}$$

Using Eqs.(6), (9), and (10) in Eq.(4), together with the various production and loss processes, we obtain a set of coupled species equations involving the densities and the electron temperature. For each positive ion species, Eq.(4) becomes

$$\frac{4D_{i,+}n_{0,i}}{l/2} = \int_0^{l/2} \left\{ k_{iz}n_{0,e}n_{n_i} - k_{rec,i}n_{0,-}n_{0,i}\left(1 - \frac{x^2}{(l/2)^2}\right)^2 \right\} dx, \tag{11}$$

where k_{iz} is the ionization rate constant, n_{n_i} is the density of the neutral species that generates the positive ion, and $k_{rec,i}$ is the rate constant for recombination with negative ions, which we assume is the dominant recombination term. For the negative ions the diffusion term is absent and k_{iz} is replaced by k_{att}. Other terms such as charge transfer are also included in the particle balance (see Tables 1–3). In the appendix, we discuss how to include the contributions from those reactions in the particle balance equations.

2.3 Power balance

The total power balance in the discharge is written as

$$P_{abs} = P_{abs,e} + P_{abs,ion}, \tag{12}$$

where $P_{abs,e}$ is the power deposited in the electrons and $P_{abs,ion}$ is the power deposited in those ions accelerated across the DC sheath potential.

The power balance of the electrons is

$$P_{abs,e} = P_{ev} + P_{ew}, \tag{13}$$

where P_{ev} is the power lost by electrons due to all electron- neutral collisions and P_{ew} is the power lost by electrons striking the wall. The average energy lost per electron striking the wall is small, $\varepsilon_{ie} \approx 2T_e$(Ref. 5). Using the energy loss ε_c per electron-ion pair created due to all electron-neutral collisions, we can write the electron power balance as

$$P_{abs,e} = A\sum_{i=1}^{r}\left(\varepsilon_{T,i}\Gamma_{i,+} + 2\int_0^{l/2} k_{rec,i} n_- n_{+,i}\varepsilon_{c,i}dx\right), \tag{14}$$

where $\varepsilon_{T,i} = \varepsilon_{c,i} + \varepsilon_{ew}$, the summation is over all positive charged species in the plasma, and $A = 2\pi R^2$ is the surface area of the discharge, ignoring the small contribution from the side surface.

The power deposited in the ions accelerated across the DC sheath potential is

$$P_{abs,ion} = eV_{DC}A\sum_{i=1}^{r}\Gamma_{i,+} = eV_{DC}A\sum_{i=1}^{r}\frac{4D_{i,+}n_{0,i}}{l/2} \tag{15}$$

where V_{DC} is the DC voltage across the sheath. In a capacitive collisional sheath model[7], the DC voltage across each sheath is related to the RF voltage across the sheath as

$$V_{DC} = 0.8V_1, \tag{16}$$

where V_1 is the fundamental RF voltage amplitude across each sheath. The RF current amplitude is related to the RF voltage as[7]

$$J_1 = 1.52\frac{\omega\epsilon_0}{s_m}V_1, \tag{17}$$

where J_1 is the RF current amplitude, ω is the RF frequency, and s_m is the sheath width.

In our model, we assume there is a single dominant positive ion species in the discharge, as will be shown in Section IV. Thus, we can approximately calculate the sheath width using the collisional Child law[5] as

$$\Gamma_{i',+} = 1.7\epsilon_0\left(\frac{2e\lambda_{i'}}{M_{i'}}\right)^{1/2}\frac{V_{DC}^{3/2}}{s_m^{5/2}}, \tag{18}$$

where i' denotes the dominant positive ion species in the discharge, $\lambda_{i'}$ is the ion mean free path, and $M_{i'}$ is the ion mass.

Solving Eqs.(16) and (17) for V_{DC} in terms of J_1 and substituting for these quantities in Eq.(18) we obtain the following expression for the sheath width, where we have substituted for $\Gamma_{i',+}$ from Eq. (9)

$$s_m = \frac{1.7(0.8)^{3/2}}{(1.52)^{3/2}\omega^{3/2}\epsilon_0^{1/2}}\left(\frac{2e\lambda_{i'}}{M_{i'}}\right)^{1/2}\frac{J_1^{3/2}}{\frac{4eD_{i',+}n_{0,i'}}{l/2}}. \tag{19}$$

Substituting Eq.(19) into Eq.(17) and using Eq. (16), we obtain the DC voltage as

$$V_{DC} = \frac{1.7(0.8)^{5/2}}{(1.52)^{5/2}\omega^{5/2}\epsilon_0^{3/2}}\left(\frac{2e\lambda_{i'}}{M_{i'}}\right)^{1/2}\frac{J_1^{5/2}}{\frac{4eD_{i',+}n_{0,i'}}{l/2}}. \tag{20}$$

The power deposited in the ions is then written in terms of the current from Eq.(15) as

$$P_{abs,ion} = \frac{1.7(0.8)^{5/2}A}{(1.52)^{5/2}\omega^{5/2}\epsilon_0^{3/2}}\left(\frac{2e\lambda_{i'}}{M_{i'}}\right)^{1/2}J_1^{5/2}. \tag{21}$$

We have replaced the summation in Eq.(15) by a single term due to the dominant ion species.

Substituting from Eqs. (14) and (21), we can write the total power balance as

$$P_{abs} = A\sum_{i=1}^{r}\left(\varepsilon_{T,i}\Gamma_{i,+} + 2\int_0^{l/2} k_{rec,i} n_- n_{+,i}\varepsilon_{c,i} dx\right) + \frac{1.7(0.8)^{5/2}A}{(1.52)^{5/2}\omega^{5/2}\epsilon_0^{3/2}}\left(\frac{2e\lambda_{i'}}{M_{i'}}\right)^{1/2} J_1^{5/2} \tag{22}$$

We calculate the RF current density by using Eq. (14) for the power balance of the electrons. Expressing $P_{abs,e}$ in terms of J_1 via Ohm's law gives

$$\frac{J_1^2}{2\sigma}V = A\sum_{i=1}^{r}\left(\varepsilon_{T,i}\Gamma_{i,+} + 2\int_0^{l/2} k_{rec,i} n_- n_{+,i}\varepsilon_{c,i} dx\right), \tag{23}$$

where V is the volume of the plasma, σ is the plasma electrical conductivity given in terms of the electron mass m and the electron-neutral collision frequency ν as

$$\sigma = \frac{n_e e^2}{m\nu}. \tag{24}$$

Together with the equations for the neutral species, the set of Eq. (11) and Eq. (22) for the power balance can be solved simultaneously for the neutral species densities, the ion species densities, and for n_e and T_e. The results, including the less important terms that we have neglected in Eqs. (11) and (14) for the sake of clarity, are given in the next section.

3 Application to Capacitive Discharges

We have applied the global model to calculate the densities of heavy species, electron density, electron temperature, RF voltage, and current, sheath width, and plasma impedance in a discharge with either chlorine gas or a mixture of chlorine and helium gases. We formulate the problem for the more general

case of chlorine/helium feedstock although the comparison with experiment will be done for pure chlorine feedstock.

Using the global model for chlorine/helium discharges, we calculate the densities for the neutral species, Cl_2, Cl, He, and metastable He^*, and the densities for the charged species, Cl_2^+, Cl^+, Cl^-, and He^+, in addition to the electron density and temperature. The electron-neutral collisions include elastic scattering, excitation, ionization, dissociation, and dissociative attachment. In addition, we include charge-transfer for ion-neutral collisions, negative-positive ion mutual neutralization, and Penning ionization of neutral chlorine atoms, molecules, and negative ions by metastable helium atoms. In Tables 1–3, we summarize the reactions included in the global model.

In Table 4, we present our numerical results for a discharge powered by a RF source of 205 W and operated at an inlet pressure of 425 mTorr and at flowrates for He and Cl_2 of 340 sccm and 160 sccm, respectively. The surface recombination coefficient for chlorine atoms is assumed to be 0.2. The densities for the charged ions presented in Table 4 are the values at the center of the discharge. The results show that the species in the discharge consist primarily of neutral chlorine molecules and helium atoms. The fraction of dissociation of chlorine molecules is approximately 6%. The densities of charged species consist mostly of Cl_2^+ and Cl^-. The density of helium ions is relatively low because of the high ionization potential of helium atoms and the low temperature in the discharge. The discharge is highly electronegative with a value of $\alpha_0 = n_{0,-}/n_{0,e} \approx 51.4$. This is consistent with the result that the fractional dissociation in the discharge is low; hence the source term for production of negative ions is large.

The most direct electrical control parameters to describe the variation of the plasma parameters are the RF power deposited in the electrons, $P_{abs,e}$, or the RF current. To investigate how the densities of the species and the electron temperature in the chlorine/helium discharge scale with inlet pressure and the RF power deposited in the electrons or the RF current, we have performed calculations by using the global model for a range of electron power densities of 0.01–0.3 Wcm^{-2} or RF currents of 10^{-3}–10^{-1} amp-cm^{-2} and pressures of 200, 425, and 600 mTorr. The results are shown in Figs. 2a–2f as a function of electron absorbed power.

The atomic and molecular chlorine ions and the negative chlorine ions are practically independent of pressure, showing a very small increase in their densities with pressure. The densities of those ions, on the other hand, increase significantly with the RF power absorbed by the electrons. However, the degree of increase with power varies differently among those ions. The atomic chlorine ions show the largest increase in density with power.

The densities of electrons and chlorine atoms increase linearly with absorbed power. However, each has a very different dependence of density on pressure. The density of chlorine atoms increases with pressure, while the density of electrons decreases with pressure.

The electron temperature is only very weakly dependent on pressure and on the RF power absorbed by the electrons. The temperature varies between 2.15 and 2.33 eV over the range of absorbed power densities of 0.1–0.3 W cm^{-2} and an inlet pressure range of 200– 600 mTorr.

As expected, the densities of chlorine molecules and helium atoms are approximately independent of the RF power absorbed by the electrons, but increase linearly with pressure. This results from the low dissociation and

ionization of chlorine molecules and the low ionization of helium atoms in the discharge. We do not show those results here.

The results presented in Figs. 2 use a surface recombination coefficient of chlorine atoms equal to 0.2, which is poorly known. Using a value of the surface recombination coefficient of 0.1, we find that the densities of chlorine atoms and ions increase approximately by a factor of two, as expected, since most of the loss of chlorine atoms is to the discharge walls. However, the change in densities of the other species and the electron temperature is at most 10%. We can understand these results in terms of the low dissociation of Cl_2 in the discharge.

In Fig. 3 we plot the RF current density versus the electron power, for the three values of pressure. The current is found to be proportional to the power and inversely proportional to the pressure. When the densities and electron temperature are plotted as a function of current, there will be new dependencies on the pressure that reflect the power and pressure dependencies of the RF current as given in Fig. 3. All the proportionalities in Figs. 2 and 3 are easily obtained from the basic equations, as obtained in the next section.

Our calculations show that the ionization and the excitation of helium atoms are very low in the discharge. Accordingly, helium atoms play a minor role in determining the charged particle balance and power balance in the discharge. To confirm the effect on the densities of chlorine species due to the presence of helium atoms, we have performed a calculation in which the rate coefficients for all the collisions between helium atoms and the chlorine species are set to zero. The results show that the densities of the chlorine species are changed by less than 3 percent. The densities of the helium ions

and metastable helium atoms, on the other hand, increase significantly due to the neglect of Penning ionizations. We conclude that helium atoms play a very minor role in determining the equilibrium parameters of the discharge. As a result, the densities of the heavy species and the electron density and temperature in a discharge containing only chlorine gas will follow the same scalings as those in Figs. 2–3.

4 Analytic Scaling Results

4.1 Scaling with pressure and RF power deposited in electrons

Using Eq.(4), for the example given in Table 4, we calculate the ratio R of positive ion diffusive loss to recombination loss to be

$$R = \frac{\frac{\sum_i 4 D_{i,+} n_{0,i}}{l/2}}{2 \sum_i \int_0^{l/2} k_{rec} n_{0,-} n_{0,i} (1 - \frac{x^2}{(l/2)^2})^2 dx} \approx 0.09 \qquad (25)$$

which indicates that the diffusive loss to the wall is of minor significance. This is true for all of the cases studied. We note, however, that for an R-value given by Eq. (25), the Boltzmann assumption is not strictly valid for the negative ions[6]. The result is that the electron density is not constrained to be uniform in the plasma. However, numerical comparison of the global model with more general analysis indicates that the parabolic profile is still a reasonable assumption.

We can therefore greatly simplify our treatment by setting the rate of production of positive ions by electron-neutral ionization equal to the rate of recombination. Accordingly, we describe the power absorbed by the electrons

in the discharge in terms of the volume recombination rate alone as

$$P_{abs,e} = V\sum_{i=1}\varepsilon_{c,i}n_{-}n_{+,i}k_{rec,i}. \tag{26}$$

Here, we do not include the profiles of the charged particles which do not affect the scalings, within our approximation that the profiles remain constant. In the following discussion, we consider only species of chlorine and electrons, as the calculations indicated that helium species played a minor role in determing the equilibrium parameters.

Since the dominant positive ion species in the discharge is Cl_2^+ and its value approximately equals the density of Cl^-, we simplify Eq.(26) to

$$P_{abs,e} = \varepsilon_c k_{rec} n_{Cl_2^+}^2 V. \tag{27}$$

Then, solving Eq.(27) for $n_{Cl_2^+}$ gives

$$n_{Cl_2^+} = n_{Cl^-} = \left(\frac{P_{abs,e}}{\varepsilon_c k_{rec} V}\right)^{1/2}. \tag{28}$$

If we neglect the weak temperature dependence of ε_c and k_{rec}, we find that the densities of Cl_2^+ and Cl^- are approximately independent of pressure and scale with power as $P_{abs,e}^{1/2}$, as shown in Figs. 2a and 2c.

For negative ions, the dominant loss process is also positive-negative ion recombination and those ions are produced by dissociative attachment. Then, the particle balance equation for negative ions takes the form

$$k_{att} n_e n_{Cl_2} = k_{rec} n_{Cl^-} n_{Cl_2^+}, \tag{29}$$

where k_{att} is the rate coefficient for dissociative attachment.

Again, setting $n_{Cl^-} = n_{Cl_2^+}$ and ignoring the weak temperature dependence, we solve Eq. (29) for n_e, and using Eq. (28) for $n_{Cl_2^+}$, we obtain

$$n_e = \frac{P_{abs,e}}{\varepsilon_c k_{att} n_{Cl_2} V}. \tag{30}$$

This shows that the electron density increases linearly with absorbed electron power. Since the neutral density n_{Cl_2} increases with the inlet pressure, the electron density scales approximately with the inverse of pressure. These scalings are seen in Fig. 2d.

In the discharge, chlorine atoms are produced primarily by dissociation of chlorine molecules and destroyed by surface recombination. The particle balance equation for Cl becomes

$$n_e n_{Cl_2} k_{diss} = n_{Cl} \gamma D_{eff} / \Lambda^2, \tag{31}$$

where γ is the surface recombination coefficient for Cl, Λ = (volume of the discharge)/(surface area of the discharge) is a diffusion scale length, and D_{eff} is an effective diffusion coefficient.

At high pressure D_{eff} has the scaling

$$D_{Cl,Cl_2} = \frac{C_0}{p}, \tag{32}$$

where p is the pressure of the discharge that is calculated based on all neutral densities and C_0 is a function of gas temperature, the masses of Cl and Cl_2, and the parameters in the intermolecular potential describing the interaction between the two species. Then, using Eq.(31) together with Eq.(30) for n_e, we find

$$n_{Cl} = \frac{k_{diss}}{k_{att}} \frac{p P_{abs,e}}{\varepsilon_c C_0}, \tag{33}$$

i.e., the density of chlorine atoms scales linearly with both pressure and electron power, as seen in Fig. 2e.

Both the positive ions Cl^+ and Cl_2^+ are created by electron impact ionization and destroyed by negative-positive ion recombination. The particle

balance equations for these ions are

$$k_{iz,Cl_2} n_e n_{Cl_2} = k_{rec} n_{Cl^-} n_{Cl_2^+}, \tag{34}$$

$$k_{iz,Cl} n_e n_{Cl} = k_{rec} n_{Cl^-} n_{Cl^+}, \tag{35}$$

where k_{iz,Cl_2} is the ionization rate coefficient of Cl_2 and $k_{iz,Cl}$ is the ionization rate coefficient of Cl. The rate coefficients for those two species are approximately equal at a given electron temperature of the discharge. Then, combining Eqs.(34) and (35), we find,

$$\frac{n_{Cl^+}}{n_{Cl}} = \frac{n_{Cl_2^+}}{n_{Cl_2}}, \tag{36}$$

1.e., the degree of ionization is the same for both Cl and Cl_2 .

Substituting Eq.(28) for $n_{Cl_2^+}$ and Eq.(33) for n_{Cl} into Eq.(36) gives

$$n_{Cl^+} = \frac{p}{n_{Cl_2}} \frac{k_{diss}}{k_{att} k_{rec}^{1/2}} \frac{P_{abs,e}^{3/2}}{\varepsilon_c^{3/2} C_0 V^{3/2}}. \tag{37}$$

Since n_{Cl_2} increases linearly with p, n_{Cl^+} becomes approximately independent of pressure and scales with absorbed electron power as $P_{abs,e}^{3/2}$, as seen in Fig. 2b.

Since the loss rates for positive and negative ions are the same within our approximation, we can combine Eq.(29) and Eq.(34), to obtain an equation for the electron temperature as

$$k_{att}(kT_e) = k_{iz,Cl_2}(kT_e). \tag{38}$$

This yields T_e=1.92 eV, which is independent of both pressure and power. The weak dependence of temperature on pressure and power as shown in Fig. 2f arises from the effects that we have neglected such as the positive ion loss to the walls.

To obtain the scaling of RF current with power absorbed by electrons and pressure, we solve Ohm's law together with Eq.(30) to obtain the current as

$$J_1 = \frac{\sqrt{2}eP_{abs,e}}{(m\nu\varepsilon_c k_{att} n_{Cl_2})^{1/2} V}, \tag{39}$$

where ν is the electron-neutral collision frequency given in terms of the rate coefficient $< v\sigma_e >$ as

$$\nu = n_{Cl_2} < v\sigma_e > . \tag{40}$$

Substituting Eq. (50) for ν into Eq. (39), we obtain

$$J_1 = \frac{\sqrt{2}eP_{abs,e}}{(m < v\sigma_e > \varepsilon_c k_{att})^{1/2} n_{Cl_2} V}. \tag{41}$$

The RF current scales linearly with power deposited in the electrons and inversely with inlet pressure as shown in Fig. 3.

We write the ion mean free path as

$$\lambda_{Cl_2^+} = \frac{1}{n_{Cl_2}\sigma_{Cl_2^+}}, \tag{42}$$

where $\sigma_{Cl_2^+}$ is the ion-neutral momentum transfer cross section. The diffusion coefficient is then expressed in terms of $\lambda_{Cl_2^+}$ as

$$D_{Cl_2^+,+} = \frac{T_i}{n_{Cl_2}\sigma_{Cl_2^+}\overline{v}M_{Cl_2}}, \tag{43}$$

where $\overline{v}$ is the average ion thermal velocity.

Substituting Eq. (28) for $n_{Cl_2^+}$, Eq. (41) for J_1, Eq. (42) for $\lambda_{Cl_2^+}$, and Eq. (43) for $D_{Cl_2^+,+}$ into Eq. (20), we have

$$V_{DC} = \frac{Al}{V^2}\frac{1.7(0.8)^{5/2}e^2}{(1.52)^{5/2}2^{5/4}\omega^{5/2}\epsilon_0^{3/2}}\frac{\overline{v}}{T_i}\left(\frac{(\sigma_{Cl_2^+}M_{Cl_2})^2}{(m < v\sigma_e >)^5(\varepsilon_c k_{att})^3}\right)^{1/4}\frac{P_{abs,e}^2}{n_{Cl_2}^2}. \tag{44}$$

The DC voltage scales with the square of power deposited in electrons and inversely with the square of pressure as seen in Fig. 4a.

Similarly, by substituting Eq. (41) for J_1 and Eq. (42) for $\lambda_{Cl_2^+}$ into Eq. (21), we obtain

$$P_{abs,ion} = \frac{A}{V^{5/2}} \frac{1.7(0.8)^{5/2}2^{7/4}e^3}{(1.52)^{5/2}\omega^{5/2}\epsilon_0^{3/2}(\sigma_{Cl_2^+}M_{Cl_2})^{1/2}(m < v\sigma_e > \varepsilon_c k_{att})^{5/4}} \frac{P_{abs,e}^{5/2}}{n_{Cl_2}^3}. \tag{45}$$

The RF current, DC voltage, and $P_{abs,ion}$ increase with RF power deposited in the electrons and decrease with inlet pressure. However, $P_{abs,ion}$ shows the largest increase with electron power and the largest decrease with pressure.

4.2 Scaling with pressure and RF current

Solving Eq. (41) for $P_{abs,e}$ in terms of J_1 and substituting the result into Eqs. (28) and (30), we obtain

$$n_{Cl^-} = n_{Cl_2^+} = \left(\frac{m\nu k_{att} n_{Cl_2}}{2\varepsilon_c}\right)^{1/4} \frac{(J_1 V)^{1/2}}{(e k_{rec})^{1/2}}, \tag{46}$$

$$n_e = \left(\frac{m\nu}{2e^2\varepsilon_c k_{att} n_{Cl_2}}\right)^{1/2} J_1. \tag{47}$$

These scalings agree with the numerical results in Figs. 2 and 3 taken together. Substituting Eqs. (42) and (43) together with Eq. (46) for the density of charged species into Eq. (20), we obtain the DC voltage in terms of the RF current as

$$V_{DC} = Al \frac{1.7(0.8)^{5/2}}{(1.52)^{5/2}2^{9/4}\omega^{5/2}\epsilon_0^{3/2}} \frac{\overline{v}}{T_i} \left(\frac{(\sigma_{Cl_2^+}M_{Cl_2})^2 \varepsilon_c k_{att}}{m < v\sigma_e >}\right)^{1/4} J_1^2. \tag{48}$$

The DC voltage scales with the square of RF current, but is independent of inlet pressure, as shown in Fig. 4b.

Substituting n_e given in Eq. (47) into Eq. (24) and the result into Eq. (22), we obtain the total absorbed RF power in terms of the current J_1 as

$$P_{abs} = V \frac{(m\nu\varepsilon_c k_{att} n_{Cl_2})^{1/2}}{2^{1/2}e} J_1 + \frac{1.7(0.8)^{5/2}A}{\omega^{5/2}\epsilon_0^{3/2}} \left(\frac{2e\lambda_{Cl_2^+}}{M_{Cl_2}}\right)^{1/2} J_1^{5/2}. \tag{49}$$

Further, substituting Eqs.(40) and (42) into Eq.(49), we express the total absorbed power in terms of RF current and inlet pressure as

$$P_{abs} = V\frac{(m < v\sigma_e > \varepsilon_c k_{att})^{1/2}}{2^{1/2}e} n_{Cl_2} J_1 + \frac{1.7(0.8)^{5/2} A}{\omega^{5/2}\epsilon_0^{3/2}} \left(\frac{2e}{M_{Cl_2} n_{Cl_2} \sigma_{Cl_2^+}}\right)^{1/2} J_1^{5/2}. \tag{50}$$

The first term represents the RF power deposited in the electrons and the second term gives the power deposited in the ions. The total absorbed power depends on the electron temperature through k_{att} and ν. However, as shown in the previous subsection (see Fig. 2f), the electron temperature varies less than 10% over the wide a range of power density and inlet pressure. Accordingly, we can neglect the temperature dependence in Eq.(50) and consider the total absorbed power to depend only on the inlet pressure and the RF current, as given explicitly in Eq.(50). To exhibit how the total absorbed power scales with current, we plot in Fig. 5 the quantity $P_{abs}/(n_{Cl_2} J_1)$ as a function of J_1. At low current density the sheath voltage is relatively small, so that the power absorbed by the electrons (ohmic heating) dominates, while at higher currents the larger sheath voltage results in increasing power deposited in ions, $\propto J_1^{5/2}$. There is also a pressure dependence. Ohmic heating being relatively more important at high pressure favors the linear term, while at low pressure the RF power is mainly deposited in the ions accelerated across the potential of the sheaths.

5 Comparison with Measurements

We apply the global model to analyze recent experiments performed with the Lam 490 etcher. The discharge in the etcher consists of two parallel plates each with a radius of approximately 10.16 cm and a gap spacing of 2 cm.

In the experiments, the Cl_2 flow rate was kept at 300 sccm while power and pressure were varied. The cylindrical discharge is essentially one dimensional, with its radius much greater than its height.

In the experiments, 13.56 MHz RF power from a generator is delivered to the discharge via a matching network[8]. The time- dependent RF current in the discharge and the RF voltage across the discharge are measured. Ignoring any nonlinear effect, we assume both the current and the voltage oscillate at the same fundamental frequency as the input power source. Thus, the phase angle between the current and the voltage is obtained from

$$\cos\varphi = \frac{\frac{1}{t_0}\int_0^{t_0}(V(t)I(t))dt}{V_{rms}I_{rms}}, \tag{51}$$

where t_0 is the cycle time, φ is the phase angle, $V(t)$ and $I(t)$ are the time-dependent voltage and current of the discharge, and V_{rms} and I_{rms} are the values of the root mean square voltage and current. The total absorbed power is given in terms of the phase angle as

$$P_{abs} = V_{rms}I_{rms}\cos\varphi. \tag{52}$$

This allows one to calculate the power delivered to the discharge by using the $V(t)$ and $I(t)$ measured in an experiment.

The actual voltage and current at the plasma boundary as used in the comparison with results from the model cannot be directly measured. The distributed network element between the plasma and the node of the measurement is characterized with network analyzers (HP 8353 A and HP 85046 A) with the chamber opened. V_{rms}, I_{rms}, and φ are then calculated from the measured values and the transmission matrix.

Two sets of experiments were performed with the Lam 490 etcher[8]. In one set the inlet pressure was kept constant at 400 mTorr and the input power

from the generator to the matching network was varied to obtain a variation in the RF power delivered to the discharge system. Taking into account the power loss in the matching network, the absorbed power in the discharge was measured in the range of 16–180 W. In the other set of experiments the power from the generator to the matching network was kept at a predetermined value of 110 W. The inlet pressure was varied from 100 to 1600 mTorr and the RF power delivered to the discharge system was measured.

To model the experiments, we assume the input parameters inlet pressure, feedstock gases and their flowrate rates, parallel plate radius, and gap spacing are given, together with either a total absorbed RF power or a RF current.

Given the RF current, we solve the electron power balance Eq. (23) together with the equations for neutral species and the set of Eqs. (11) for charged species to obtain the densities of heavy species, electron density, and electron temperature. The total absorbed RF power is calculated according to Eq. (22).

When the total absorbed RF power is specified instead of the RF current, we solve Eq. (22) together with the equations for neutral species and the set of Eqs. (11) for charged species to obtain the densities of heavy species, electron density, and electron temperature. The RF current is then obtained from Eq. (23).

To calculate the voltage across the discharge, we represent the discharge by an impedance model. The fundamental equivalent circuit models the two major regions of the discharge, the bulk and the two sheath regions at the plates. The bulk plasma region is described by the linear elements resistance R_p, capacitance C_p, and inductance L_p, while the two sheath regions are described by the nonlinear elements sheath resistance R_s, and sheath

capacitance C_s. The effect of the sheath inductance on the voltage across the discharge is assumed small.

The plasma capacitance calculated for a one dimensional parallel plate model is

$$C_p = \epsilon_0 \frac{A/2}{l} \approx \epsilon_0 \frac{A/2}{d - s_{m,t}}, \tag{53}$$

where $A/2$ is the surface area of each plate, assuming a symmetric discharge, d is the separation of the two plates, and $s_{m,t}$ is the total width of the two sheaths. In a high pressure discharge with strong electronegativity, the sheath is very small and $l \approx d$. Both the plasma resistance and plasma inductance are expressed in terms of C_p as[5]

$$R_p = \frac{\nu}{\omega_{p,e}^2 C_p} \tag{54}$$

and

$$L_p = \frac{1}{\omega_{p,e}^2 C_p}, \tag{55}$$

where $\omega_{p,e}$ is the electron plasma frequency.

The capacitance of the two sheaths in series combination is also approximately a linear element and is written as[5]

$$C_s = 0.76 \epsilon_0 \frac{A/2}{s_{m,t}}. \tag{56}$$

In the global model we approximate $s_{m,t}$ by s_m given in Eq. (19).

The sheath resistance R_s is calculated using the power balance equation which is rewritten as

$$P_{abs} = \frac{J_1^2}{2\sigma} V + \frac{2R_s (J_1 A)^2}{2}. \tag{57}$$

We calculate the voltage across the discharge by solving the following equation for the circuit.

$$\frac{Q_s(t)}{C_s} + L_p \frac{dI(t)}{dt} + (2R_s + R_p) I(t) = V(t), \tag{58}$$

where $Q_s(t)$ is the charge accumulated on the plate and $I(t)$ and $V(t)$ are time time-dependent current and voltage of the discharge. Writing $I(t) = I_{rms}\cos(\omega t)$ and $V(t) = V_{rms}\cos(\omega t + \varphi)$ and solving Eq. (58) gives

$$V_{rms} = I_{rms}\left((2R_s + R_p)^2 + \left(\frac{1}{\omega C_s} - \omega L_p\right)^2\right)^{1/2} \tag{59}$$

and

$$\tan\varphi = -\frac{\frac{1}{\omega C_s} - \frac{\omega}{\omega_{p,e}^2 C_p}}{2R_s + R_p}. \tag{60}$$

In Figs. 6a–6c, we compare the rms RF current and voltage and the phase angle versus inlet pressure from the global model to the data[8]. In these experiments the input power from the generator to the matching network was kept constant at a predetermined value of 110 W. In Figs. 7a–7c, we compare the rms RF current and voltage and the phase angle versus total absorbed power from the global model to the data[8]. In these experiments the inlet pressure was kept constant at 400 mTorr and the input power from the generator to the matching network was varied to produce a variation in absorbed power from 16 to 180 W. All of the data presented in Figs. 6–7 were from the experiments performed with a Lam 490 etcher.

The comparisons between the results from the global model and the measurements clearly show reasonable agreement especially on the scalings with inlet pressure and power. The general trends can be qualitatively understand in the following way. At high pressures, the electron power absorption due to ohmic heating dominates the ion power absorption in the sheaths. Hence, the first term on the right hand side of Eq. (50) dominates and $P_{abs} \propto p_{in} J_1$. At constant absorbed power, the current is inversely proportional to pressure at high pressure as seen in Fig. 6a. Although in the experiment only the input power was kept constant, the absorbed power was found to be fairly

constant at high pressure. At low pressure, the second term in Eq. (50) becomes important, leading to a weaker dependence of J_1 on p_{in}.

As Fig. 6c indicates, the phase angle between the total RF voltage and the RF current changes from resistive at high pressures to capacitive at low pressures. At high pressures the RF voltage is mainly dropped resistively across the bulk plasma. Using Eq. (59), we obtain $V_{rms} \simeq I_{rms} R_p$. Then, by using Eq. (50) together with the scaling for n_e, we obtain $V_{RF} \propto p_{in}$, as seen at high pressures in Fig. 6b. At low pressures, since the discharge is capacitive, we obtain $V_{rms} \simeq 2R_s I_{rms}$ from Eq. (59). Then, solving Eqs. (50) and (57) to obtain R_s in terms of the current gives $V_{rms} \propto P_{abs}/p_{in}^{1/5}$. This shows the voltage scales inversely with pressure at low pressures.

For the fixed pressure data of Fig. 7, we are in the ohmic heating regime such that, from Eq. (50) $J_1 \propto P_{abs}/p_{in}$, as seen in Fig. 7a. At high powers, the discharge is capacitive and $V_{rms} \simeq V_{DC} \propto J_1^2$ from Eq. (48). Using $J_1 \propto P_{abs}/p_{in}$, we see that $V_{rms} \propto (P_{abs}/p_{in})^2$ which agrees qualitatively with Fig. 7b. At low powers, the discharge is resistive and this yields $V_{rms} \propto p_{in}$, independent of P_{abs}, as also seen in Fig. 7b.

In general the agreement of the current is much better than the agreement of the voltage. For the voltage, there are significant disagreements between our results and the data at low inlet pressure, $p_{in} < 200$ mTorr, at high inlet pressure, $p_{in} > 1$ Torr, and at high absorbed RF power, $P_{abs} > 200$ W. Some of the disagreement between our results and the data might be attributed to the assumption of a symmetric discharge in our model, since the discharges in the Lam 490 etcher is not strictly symmetric. Furthermore, as the pressure decreases the collisional sheath model used in our calculation predictes an increasing sheath width such that at $p_{in} = 100$mTorr is 1 cm, compara-

ble to the gap spacing of only 2 cm. This model also assumes a constant diffusion coefficient and mobility, which is not valid at low pressures[5]. At pressures above one Torr, nonlocal ionization of the neutral species by the strong electric field in the sheath regions becomes important and secondary electron emission from the plates may also become important. Taking these effects into account in the global model would result in a lower voltage than currently predicted by the model, thereby agreeing better with the data.

6 Conclusion

We have developed a global model for high pressure (0.1–1 Torr) electronegative radio frequency (RF) discharges and applied it to molecular gases consisting of either pure chlorine species or a mixture of chlorine and helium species. The charged and neutral heavy particle densities together with the electron density and electron temperature are calculated by using the equations of particle balance and power balance for the input discharge parameters RF power or RF current, inlet pressure, gas flowrates, reactor diameter, and gap spacing. The power is assumed deposited in the electrons via ohmic heating and in those ions accelerated across the DC sheath potential. The voltage across the sheath is calculated self consistently with the densities and the electron temperature by using a collisional Child law sheath model. Our results show that the discharge is highly electronegative with a value of $\alpha_0 = n_{0,-}/n_{0,e}$ greater than 50. The fractional dissociation of chlorine molecules is less than 6%. The densities of charged species consist mostly of Cl_2^+ and Cl^-. Those ions are mainly lost in the discharge as a result of negative-positive ion recombination rather than diffusion loss to the walls.

The helium atoms in the chlorine/helium discharges play a minor role in determining the densities of charged chlorine particles, the electron density, and electron temperature. Analytic scaling laws for the dependence of the charged and neutral particle densities, electron temperature, RF voltage and current, sheath width, and plasma impedance on pressure and absorbed RF power are derived and used to explain the numerical results obtained from the global model. We have compared results from the global model to recent experimental measurements on a Lam 490 etcher, using chlorine feedstock gas. We found reasonable agreement between calculation and measurement, over a wide range of pressures and powers. In our calculations, we have not made any attempt to adjust the parameters in the model to fit the measurements.

Acknowledgements

The authors thank Dr. Chris Lee for guidance on development of the global model. This work was partially supported by NSF Grant ECS- 9217500, DOE Grant DE-FG03-87ER13727, LLNL Grant W-7405-ENG- 48, and a gift from Lam Research. This work was done during one of the authors' (YTL) leave from Lawrence Livermore National Laboratory.

Reference

1. Lam Research, "Autotech," *Operations and Maintenance Manuals*, vol. **1** & **2**, revision 9, 1994.

2. C. Lee, D. B. Graves, M. A. Lieberman, and D. W. Hess, *J. Electrochem. Soc.* **141**, 1546, 1994.

3. C. Lee and M. A. Lieberman, *J. Vac. Sci. Technol.* **A 13**, 368, 1995.

4. A. J. Lichtenberg, V. Vahedi, M. A. Lieberman, and T. Rognlien, *J. Appl. Phys.* **75**, 2339, 1994.

5. M. A. Lieberman and A. J. Lichtenberg, *Principles of Plasma Discharges and Materials Processing*, Section 10.3, Wiley Interscience, New York, 1994.

6. A. J. Lichtenberg, Y. T. Lee, M. A. Lieberman, I. Kaganovich, and L. Tsendin, to be submitted to *Plasma Sources, Sci. & Technol.*, 1996.

7. M. A. Lieberman, *IEEE Trans. Plasma Sci.* **17**, 338, 1989.

8. F. Bose, "Diagnostics and Control of Plasma Etching Reactors for Semiconductor Manufacturing", Ph. D. Dissertation, ETH No: 11224, 1995.

9. M. V. Kurepa and d. S. Belie, *J. Phys. B: Atom. Molec. Phys.*, **11(21)**, 3719, 1978.

10. P. C. Cosby and H. Helm, SRI Report, PYU 1147/MP 92- -280, 1992.

11. M. A. Lennon, K. L. Bell, H. B. Gilbody, J. G. Hughes, A. E. Kingston, M. J. Murray, and F. J. Smith, *J. Phys. Chem. Ref. Data*, **17(3)**, 1285, 1988.

12. G. L. Rogoff, J. M. Kramer, and R. B. Piejak, *IEEE Trans. Plasma Sci.*, **14(2)**, 103, 1986.

13. Estimated from similar cross section for F^- given in the paper: P. Peart, R. Forrest, and K. T. Dolder, *J. Phys.*, **B12**, L115, 1979.

14. $D_{Cl_2^+}$ estimated with the cross section for charge transfer reaction of Cl_2^+ and Cl_2.

15. D_{Cl^+} estimated with the cross section for charge transfer reaction of Cl^+ and Cl.

16. K. L. Bell, H. B. Gilbody, J. G. Hughes, A. E. Kingston, and F. J. Smith, *J. Phys. Chem. Ref. Data*, **12 (4)**, 891, 1983.

17. K. A. Berrington, P. G. Burke, L. C. G. Freitas, and A. E. Kingston, *J. Phys. B: Atom. Molec. Phys.*, **18**, 4135, 1985.

18. The de-excitation rate coefficient is calculated from detailed balancing.

19. A. J. Dixon, M. F. A. Harrison, and A. C. H. Smith, *J. Phys. B: Atom. Molec. Phys.*, **9**, 2617, 1976.

20. Estimated from similar reactions for He^* and Ar given in the paper: W. Lindinger, A. L. Schmeltekopf, and F. C. Fehsenfeld, *J. Chem. Phys.*, **61**, 2890, 1974.

21. D_{He^+} estimated with the cross section for charge transfer reaction of He^+ and He.

22. Estimated from similar reactions for O^- and O^+ given in the paper: T. D. Gaily and M. F. A. Harrison, *J. Phys.*, **B2**, L25, 1970.

Table Ia: Chlorine reactions

Number	Reaction
1	$e + Cl_2 = 2e + Cl_2^+$
2	$e + Cl_2 = e + 2Cl$
3	$e + Cl_2 = Cl + Cl^-$
4	$e + Cl = 2e + Cl^+$
5	$Cl^- + Cl_2^+ = Cl + Cl_2$
6	$Cl^- + Cl^+ = 2Cl$
7	$e + Cl^- = 2e + Cl$
8	$e + Cl_2 = e + Cl^- + Cl^+$
9	$e + Cl_2 = 2e + Cl + Cl^+$
10	$2Cl + wall = Cl_2$
11	$Cl^+ + wall = Cl$
12	$Cl_2^+ + wall = Cl_2$

Table Ib: Rate coefficients for chlorine reactions

Number	Rate Coefficients (cm^3/s)	References
1	$9.214 \times 10^{-8} e^{-12.9/T_e}$	11
2	$3.802 \times 10^{-8} e^{-3.824/T_e}$	12
3	$3.69 \times 10^{-10} \mathrm{Exp}(\sum_{i=1}^{5} a_i/T_e^i)$, $a_1 = -1.68$, $a_2 = 1.457$, $a_3 = -0.44$, $a_4 = 0.0572$, $a_5 = -0.0026$	11
4	$(T_e/12.96)^{1/2} e^{-12.96/T_e} \sum_{i=0}^{5} a_i (\log(T_e/12.96))^i$, $a_0 = 1.419 \times 10^{-7}$, $a_1 = -1.864 \times 10^{-8}$, $a_2 = -5.439 \times 10^{-8}$, $a_3 = 3.306 \times 10^{-8}$, $a_4 = -3.54 \times 10^{-9}$, $a_5 = -2.915 \times 10^{-8}$	13
5	5.0×10^{-8}	14
6	5.0×10^{-8}	14
7	$2.627 \times 10^{-8} e^{-5.375/T_e}$	15
8	$8.549 \times 10^{-10} e^{-12.65/T_e}$	11
9	$3.881 \times 10^{-8} e^{-15.5/T_e}$	11
10	γk_{loss}	2
11	$2D_{Cl_2^+} 4n_{Cl_2^+}/l$	16
12	$2D_{Cl^+} 4n_{Cl^+}/l$	17

Table IIa: Helium reactions

Number	Reaction
13	$e + He = 2e + He^+$
14	$e + He = e + He(2^1S)$
15	$e + He = e + He(2^3S)$
16	$e + He^* = e + He$
17	$e + He^* = 2e + He^+$
18	$He^* + He^* = e + He + He^+$
19	$He^+ + wall = He$

Table IIb: Rate coefficients for helium reactions

Number	Rate Coefficients (cm^3/s)	References
13	$e^{-24.60/T_e}(T_e/24.60)^{1/2}\sum_{i=0}^{5} a_i(\log(T_e/24.60))^i$,	18
	$a_0 = 1.4999 \times 10^{-8}$	
	$a_1 = 5.6656 \times 10^{-10}$	
	$a_2 = -6.0821 \times 10^{-9}$	
	$a_3 = -3.5894 \times 10^{-9}$	
	$a_4 = 1.5529 \times 10^{-9}$	
	$a_5 = 1.3207 \times 10^{-9}$	
14	$\mathrm{Exp}(\sum_{i=0}^{4} a_i(\log(T_e))^i)$,	19
	$a_0 = -40.246$	
	$a_1 = 21.959$	
	$a_2 = -10.608$	
	$a_3 = -0.569$	
	$a_4 = 1.722$	
15	$\mathrm{Exp}(\sum_{i=0}^{4} a_i(\log(T_e))^i)$,	19
	$a_0 = -18.769$	
	$a_1 = -19.987$	
	$a_2 = -0.699$	
16	$(k_{14} + 3k_{15})e^{20.0/T_e}/4$	20
17	$7.54 \times 10^{-8} e^{-4.05/T_e}$	21
18	6.2×10^{-10}	22
19	$2D_{He^+}4n_{He^+}/l$	23

Table IIIa: Reactions between chlorine and helium

Number	Reaction
20	$He^+ + Cl^- = He + Cl$
21	$He^* + Cl_2 = He + 2Cl$
22	$He^* + Cl_2 = e + He + Cl_2^+$
23	$He^* + Cl = e + He + Cl^+$
24	$He^* + Cl^- = e + He + Cl$

Table IIIb: Rate coefficients for reactions between chlorine and helium

Number	Rate Coefficient (cm^3/s)	Reference
20	2.0×10^{-7}	24
21	6.2×10^{-10}	20
22	2.7×10^{-7}	20
23	5.8×10^{-11}	20
24	1.2×10^{-11}	20

$$n_{e0} = 1.20 \times 10^{10}\text{cm}^{-3}$$

$$n_{Cl_2^+} = 5.80 \times 10^{11}\text{cm}^{-3}$$

$$n_{Cl^+} = 4.80 \times 10^{10}\text{cm}^{-3}$$

$$n_{Cl^-} = 6.16 \times 10^{11}\text{cm}^{-3}$$

$$n_{He^+} = 3.16 \times 10^{8}\text{cm}^{-3}$$

$$n_{Cl_2} = 3.82 \times 10^{15}\text{cm}^{-3}$$

$$n_{Cl} = 5.00 \times 10^{14}\text{cm}^{-3}$$

$$n_{He} = 8.66 \times 10^{15}\text{cm}^{-3}$$

$$n_{He^*} = 1.41 \times 10^{7}\text{cm}^{-3}$$

$$T_e = 2.18\text{eV}$$

Table IV: Densities and electron temperature

Input parameters: absorbed RF power is 205 W, inlet pressure is 425 mTorr, flowrates for Cl_2 and He are 340 sccm and 160 sccm, respectively, discharge radius is 11.25 cm, and gap spacing is 0.9 cm

Figure Captions

Fig. 1. Schematic drawing of the cross section of the discharge. l_s is the gap spacing of the discharge and l_p is the height of the plasma column in the discharge. $l/2$ is the profile scale length for the heavy species which is assumed to be equal to $l_s/2$.

Fig. 2. Molecular chlorine ion density (a), atomic chlorine ion density (b), negative chlorine ion density (c), electron density (d), atomic chlorine density (e), and electron temperature (f) versus absorbed power density deposited in the electrons. The dashed, solid, and dotted lines correspond to the inlet pressures of 200, 425, and 600 mTorr, respectively.

Fig. 3. RF current density versus power density deposited in the electrons. The dashed, solid, and dotted lines correspond to the inplet pressures of 200, 425, and 600 mTorr, respectively.

Fig. 4. DC voltage versus (a) power density deposited in the electrons and inlet pressure and (b) RF current density and inlet pressure. The dashed, solid, and dotted lines correspond to the inlet pressures of 200, 425, and 600 mTorr, respectively.

Fig. 5. Total absorbed RF power versus current density and inlet pressure. The dashed, solid, and dotted lines correspond to the inlet pressures of 200, 425, and 600 mTorr, respectively.

Fig. 6. J_{rms} (a), V_{rms} (b), and phase angle (c) versus inlet pressure from the global model (solid line) compared to data (solid square) obtained with the Lam 490 etcher. The input power is fixed in the experiment.

Fig. 7. J_{rms} (a), V_{rms} (b), and phase angle (c) versus absorbed power from the global model (solid line) compared to data (solid square) obtained with

the Lam 490 etcher. The solid and dotted curves correspond to the inlet pressure of 400 and 600 mTorr, respectively.

Fig. 1.

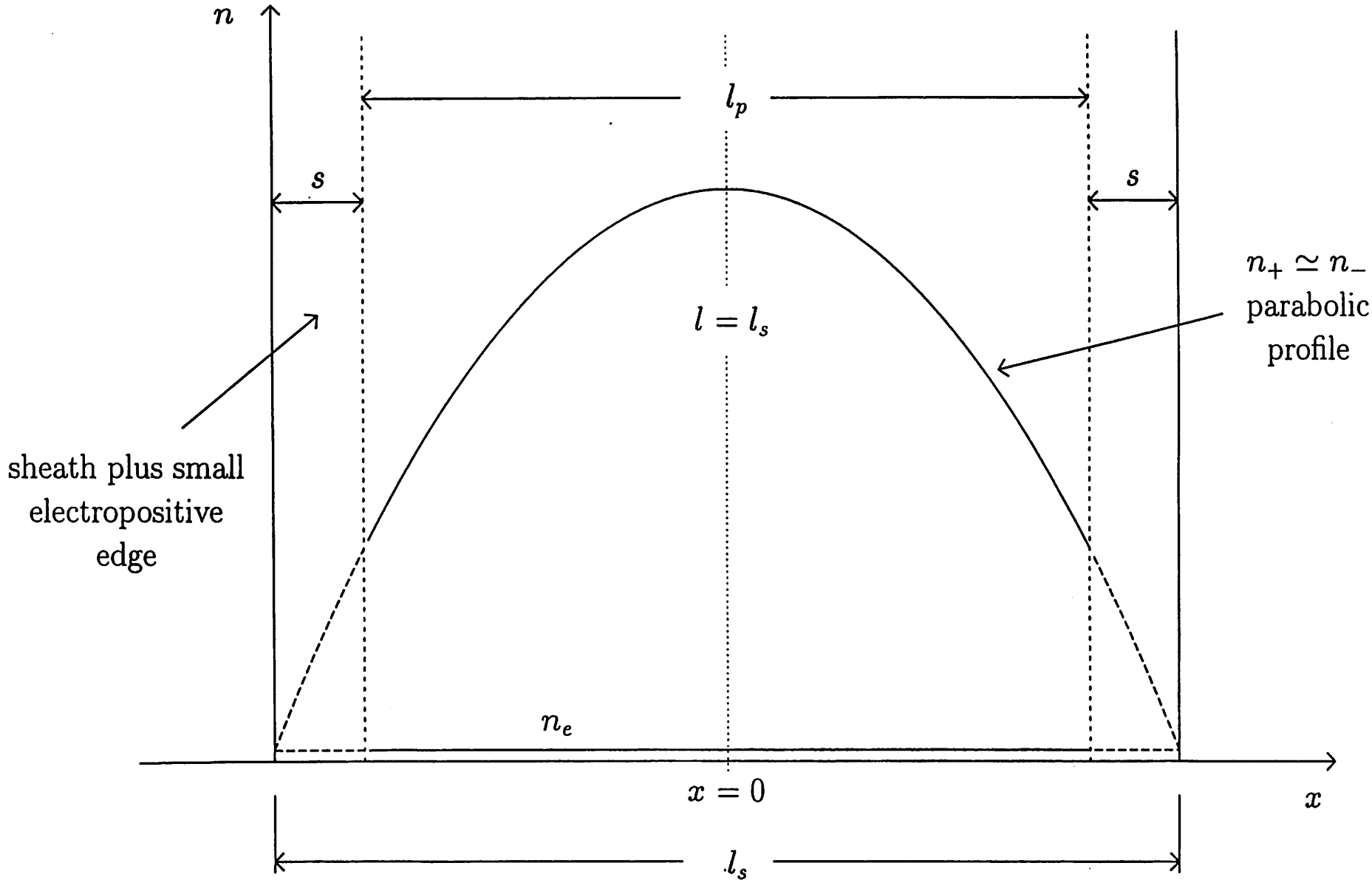
n
l_p
s
s
$n_+ \simeq n_-$
parabolic
profile
$l = l_s$
sheath plus small
electropositive
edge
n_e
$x = 0$
x
l_s

Fig. 2a: Molecular Chlorine Ion

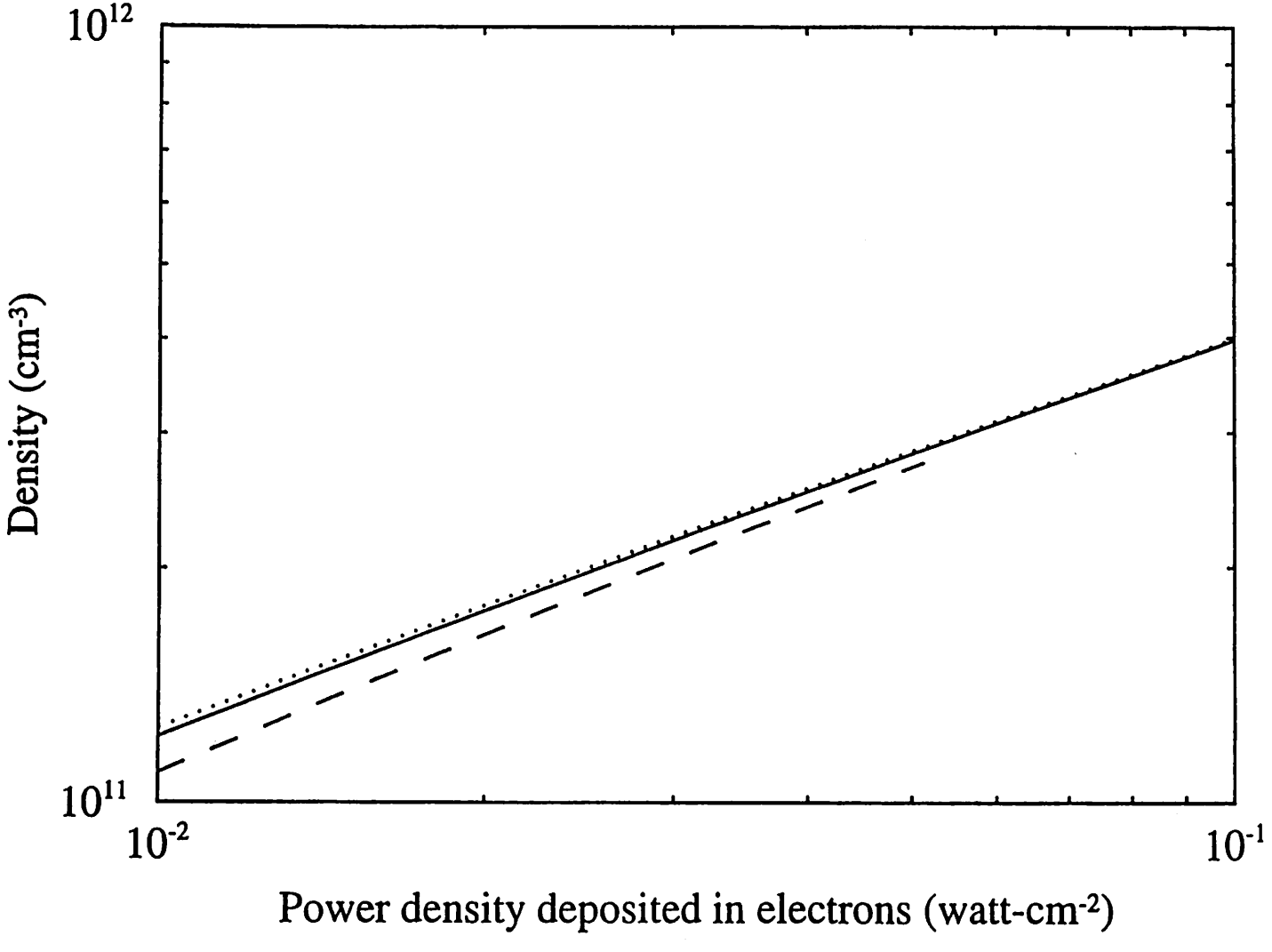

Fig. 2b: Atomic Chlorine Ion

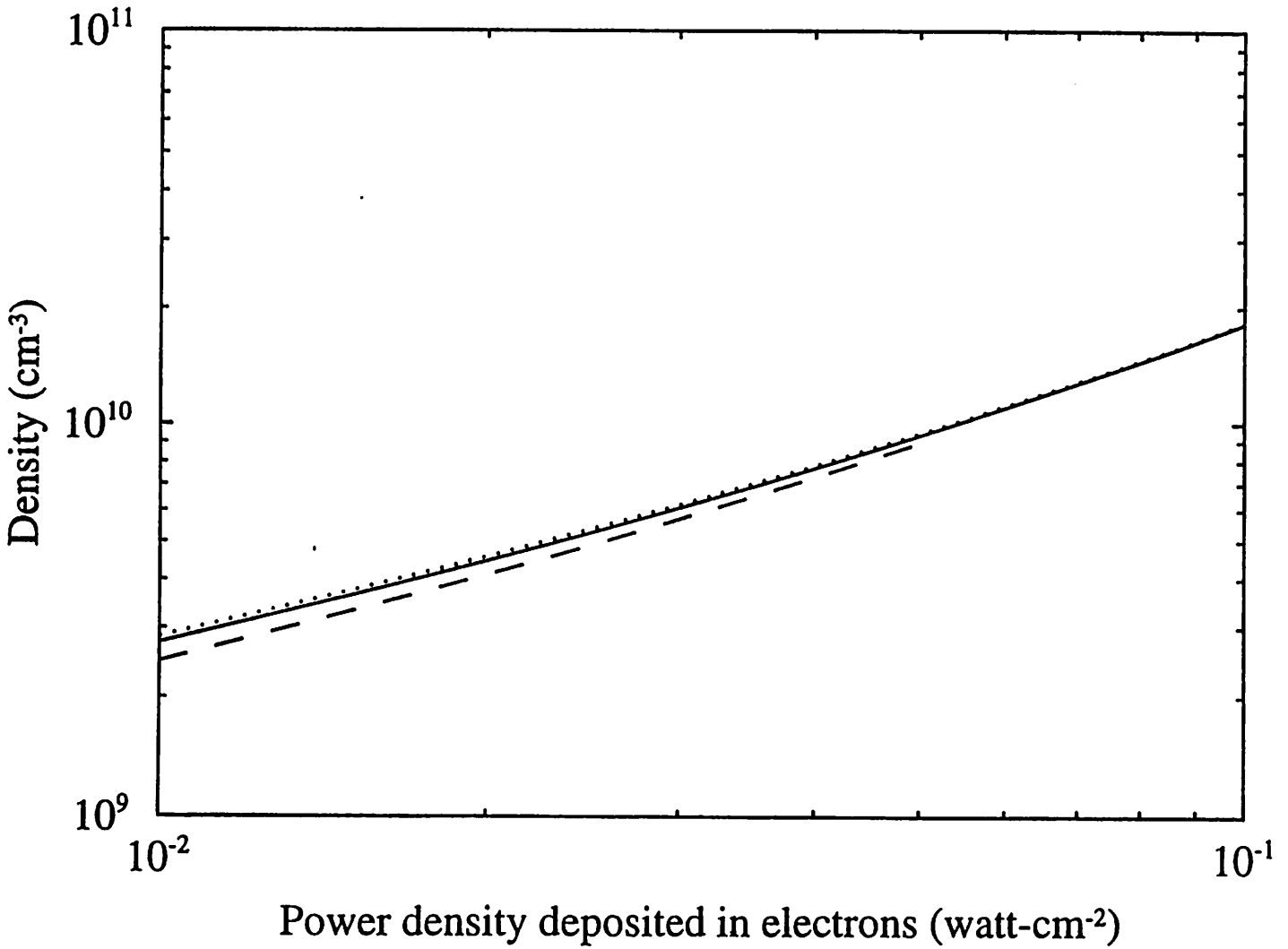

Fig. 2c: Negative Chlorine Ion

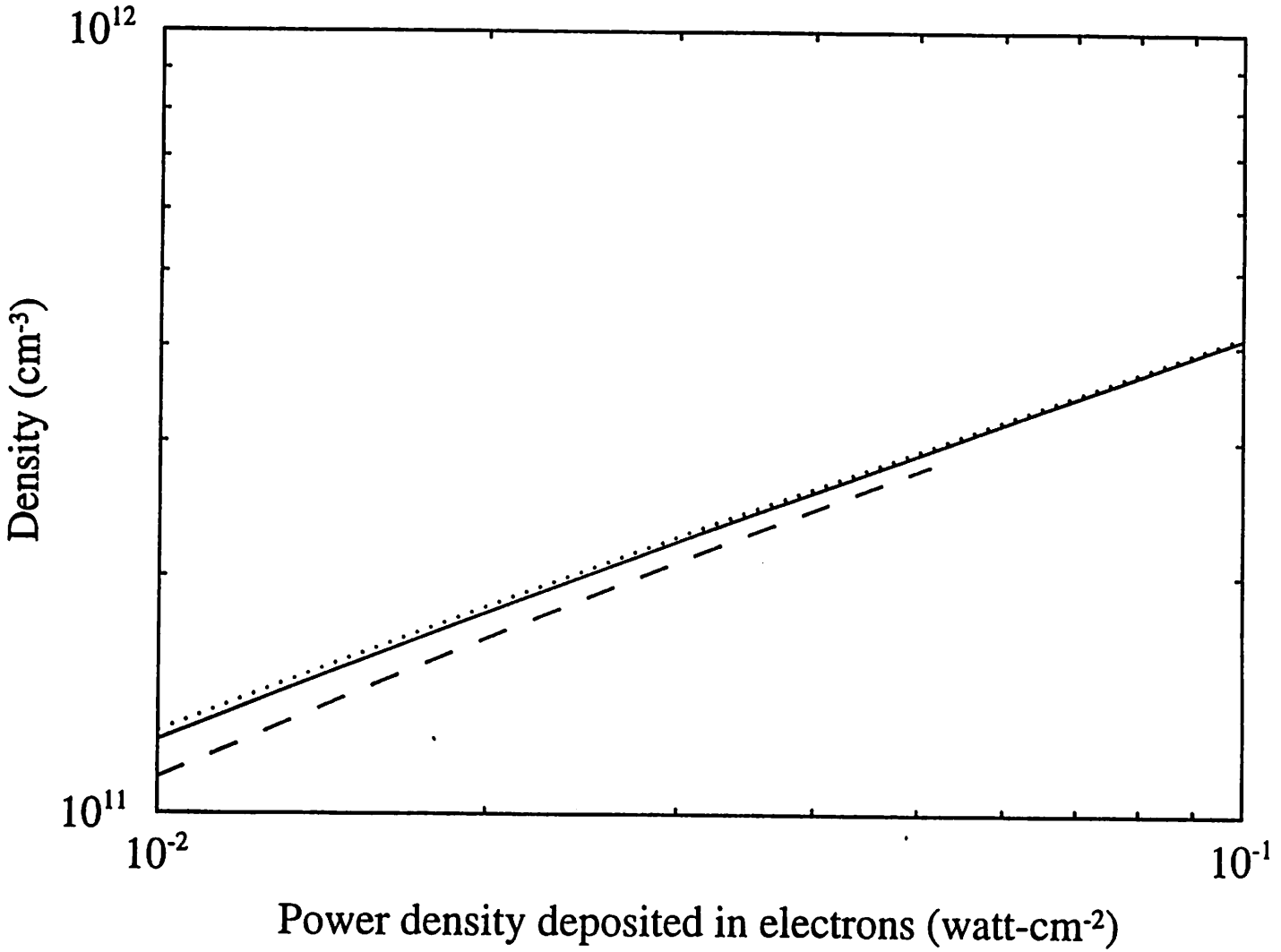

Fig. 2d: Electron Density

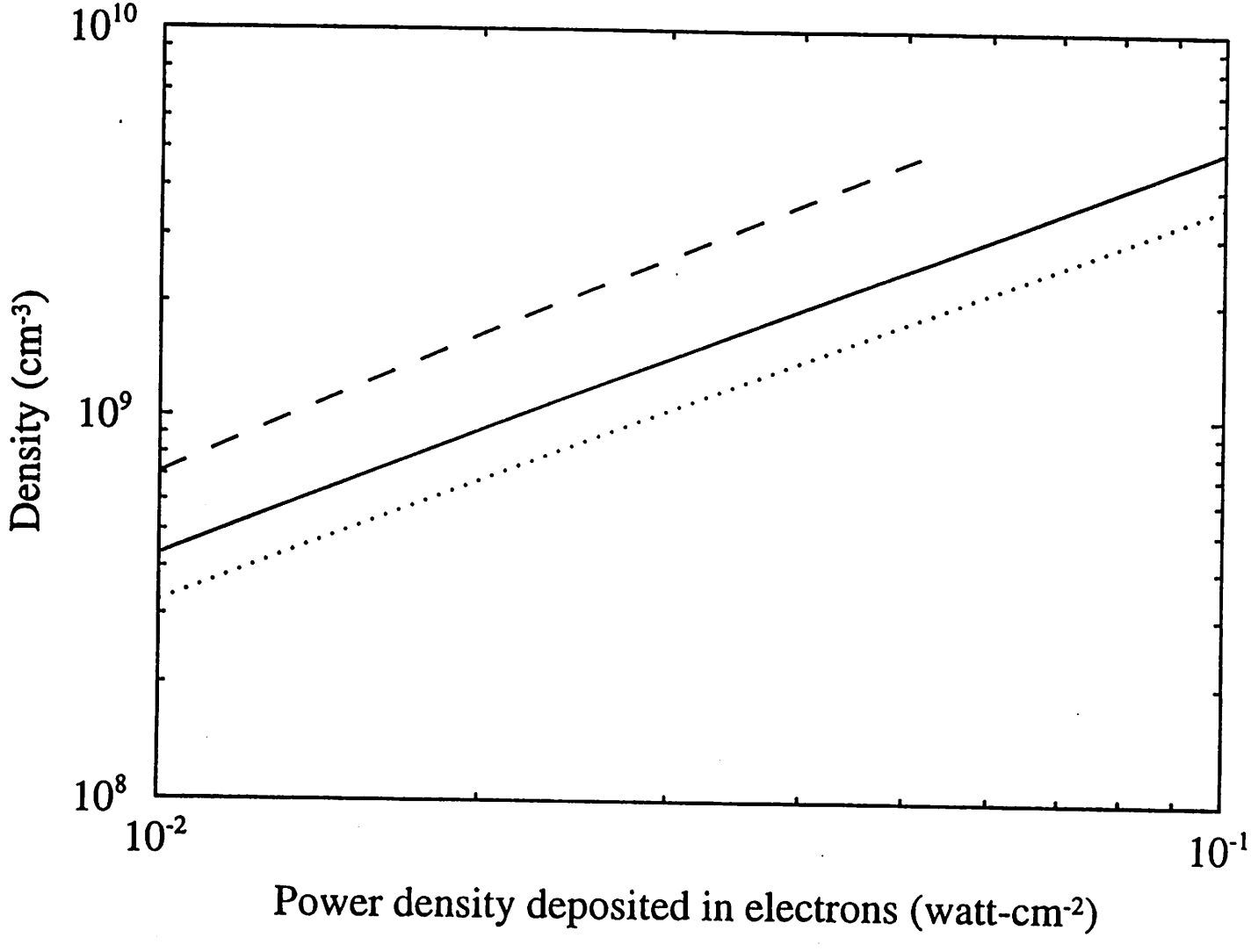

Fig. 2e: Atomic Chlorine

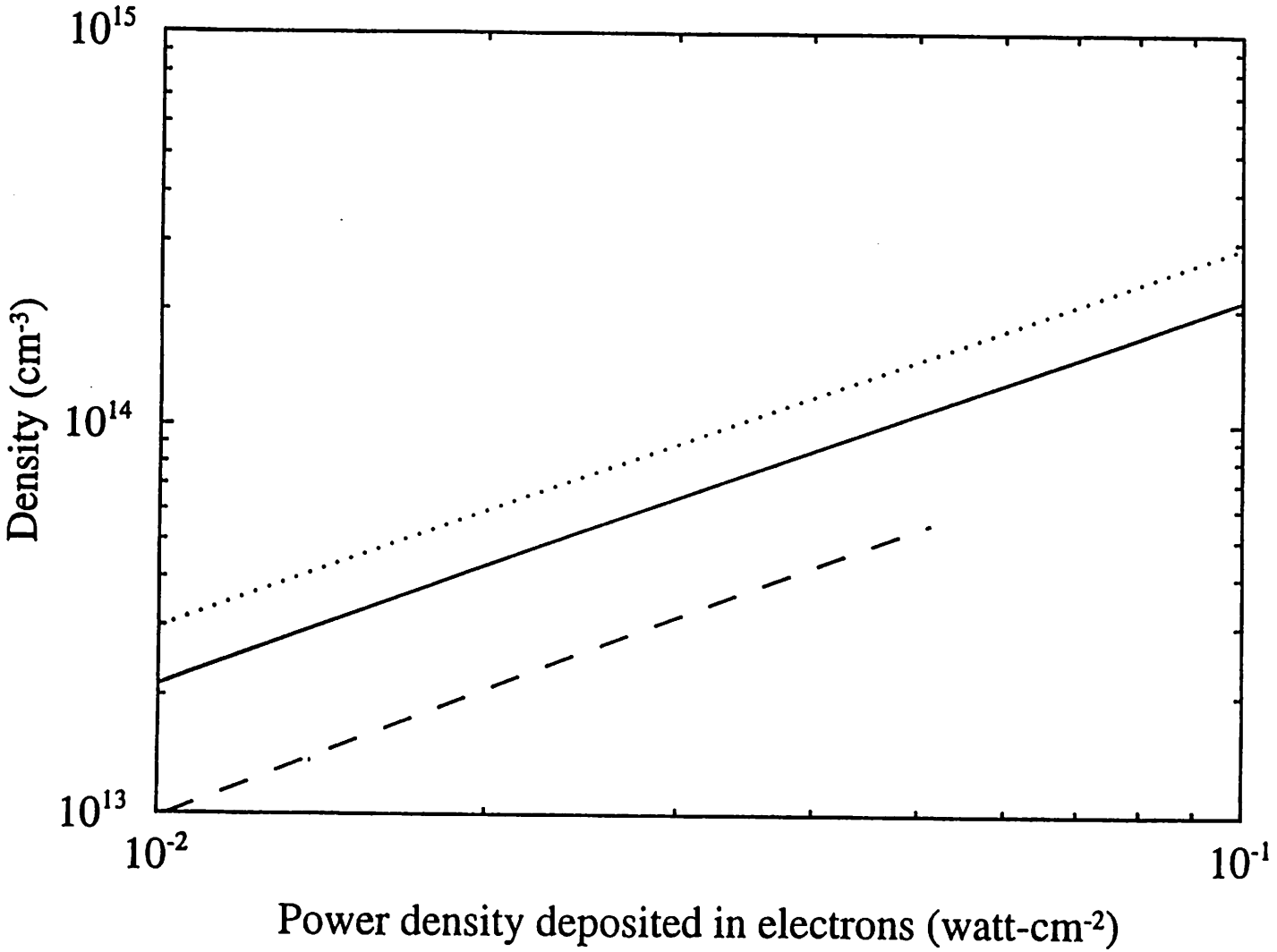

Fig. 2f: Electron Temperature

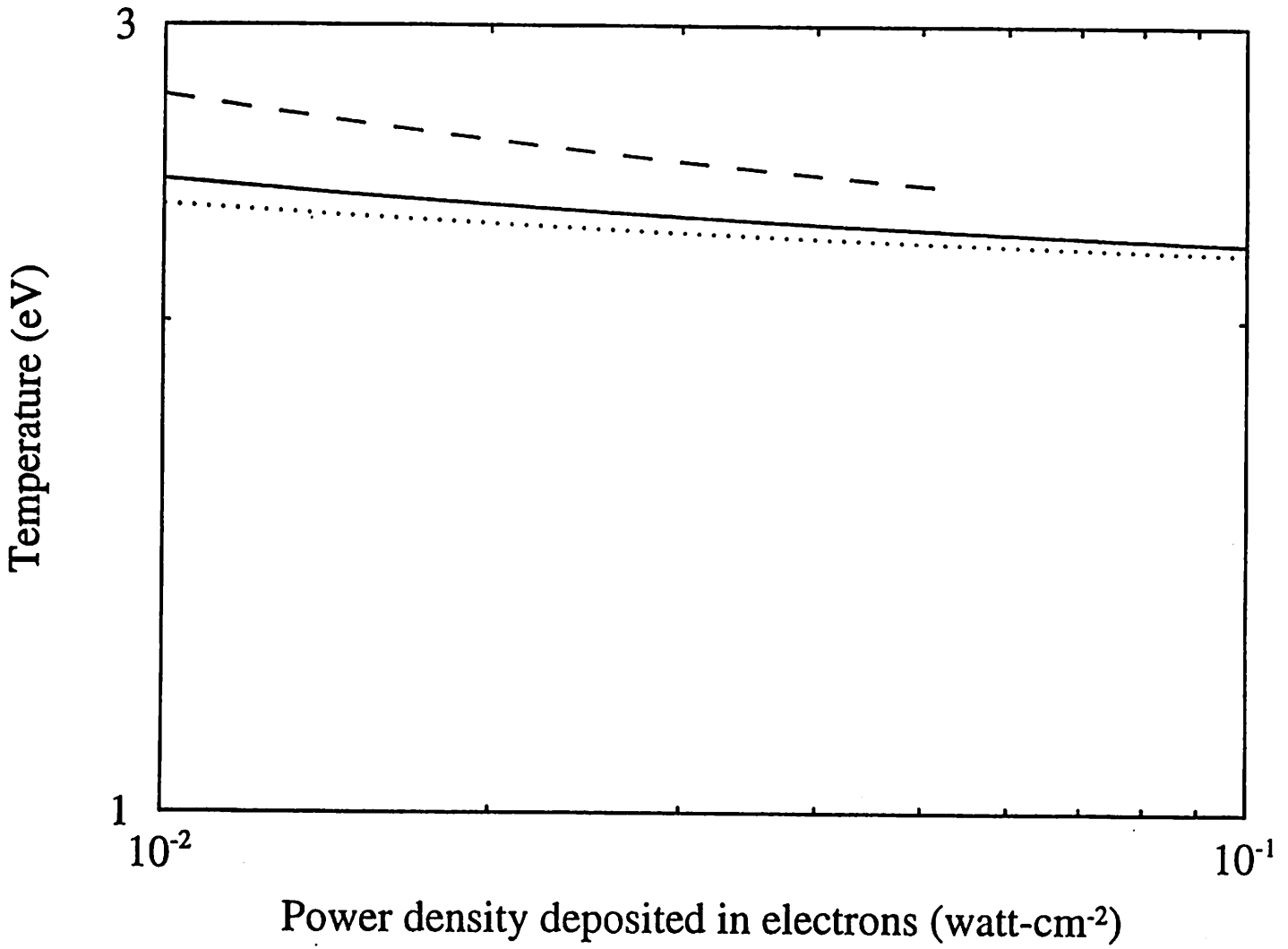

Fig. 3: RF Current Density

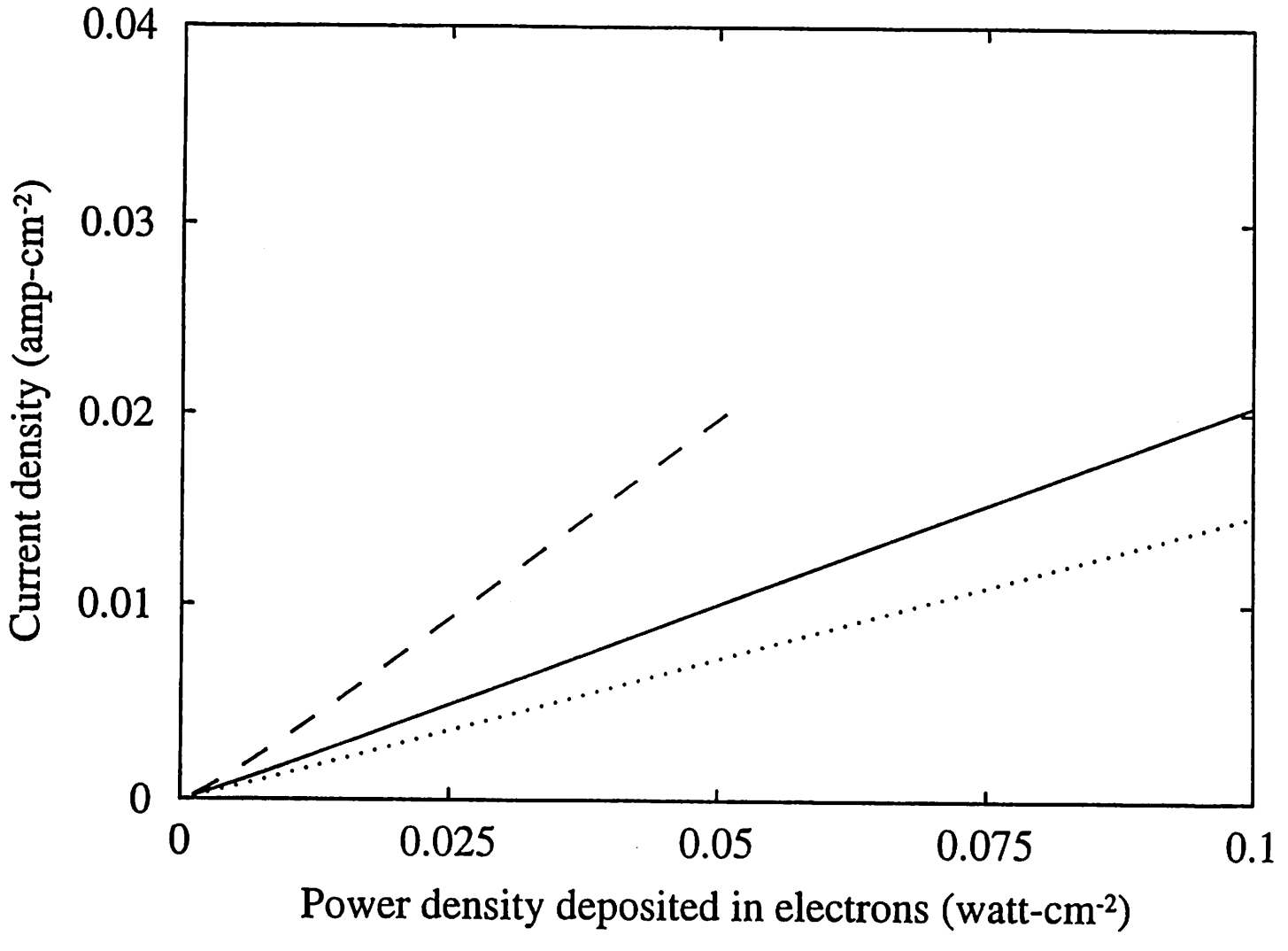

Fig. 4a: DC voltage across each sheath

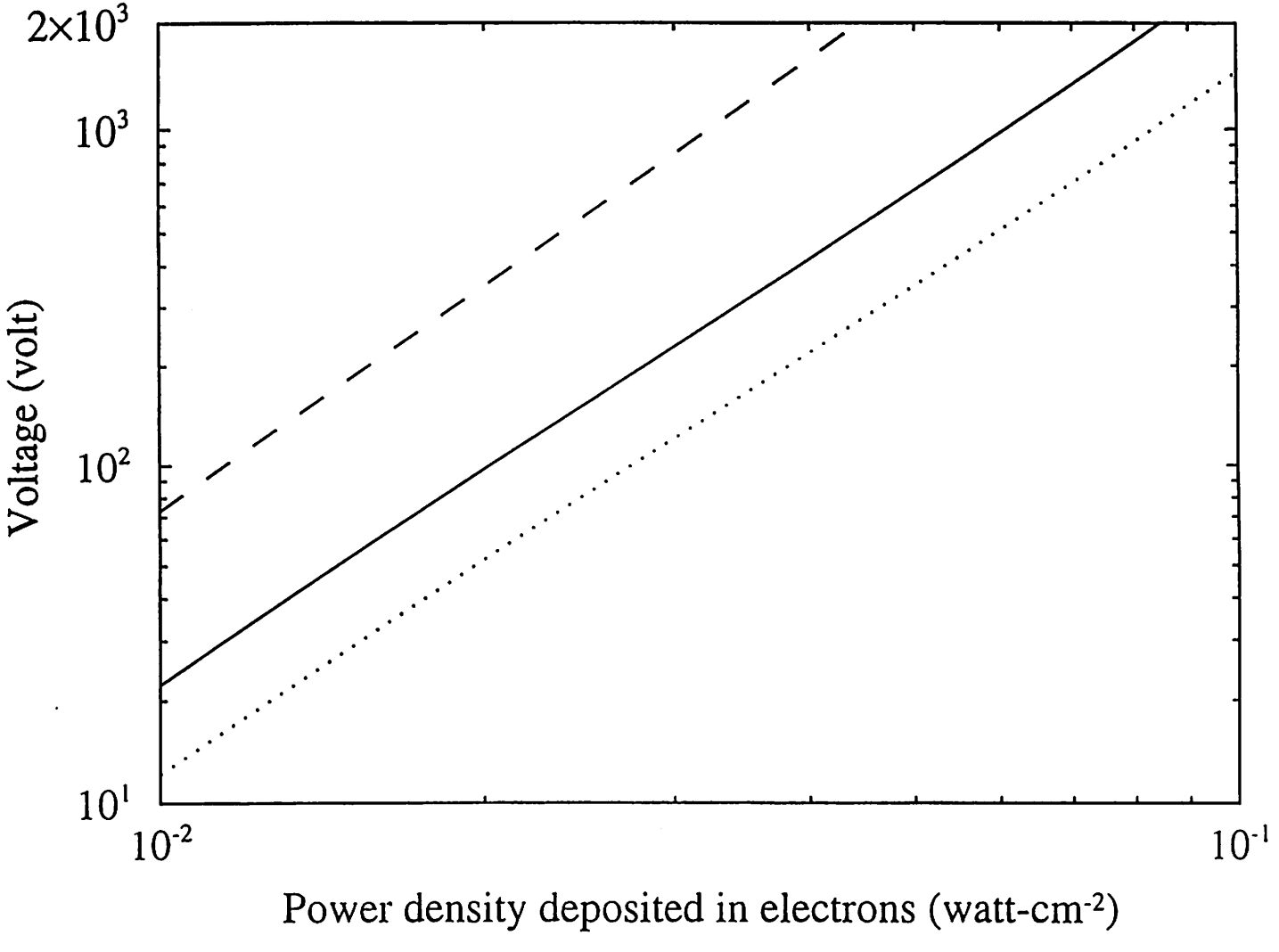

Fig. 4b: DC voltage across each sheath

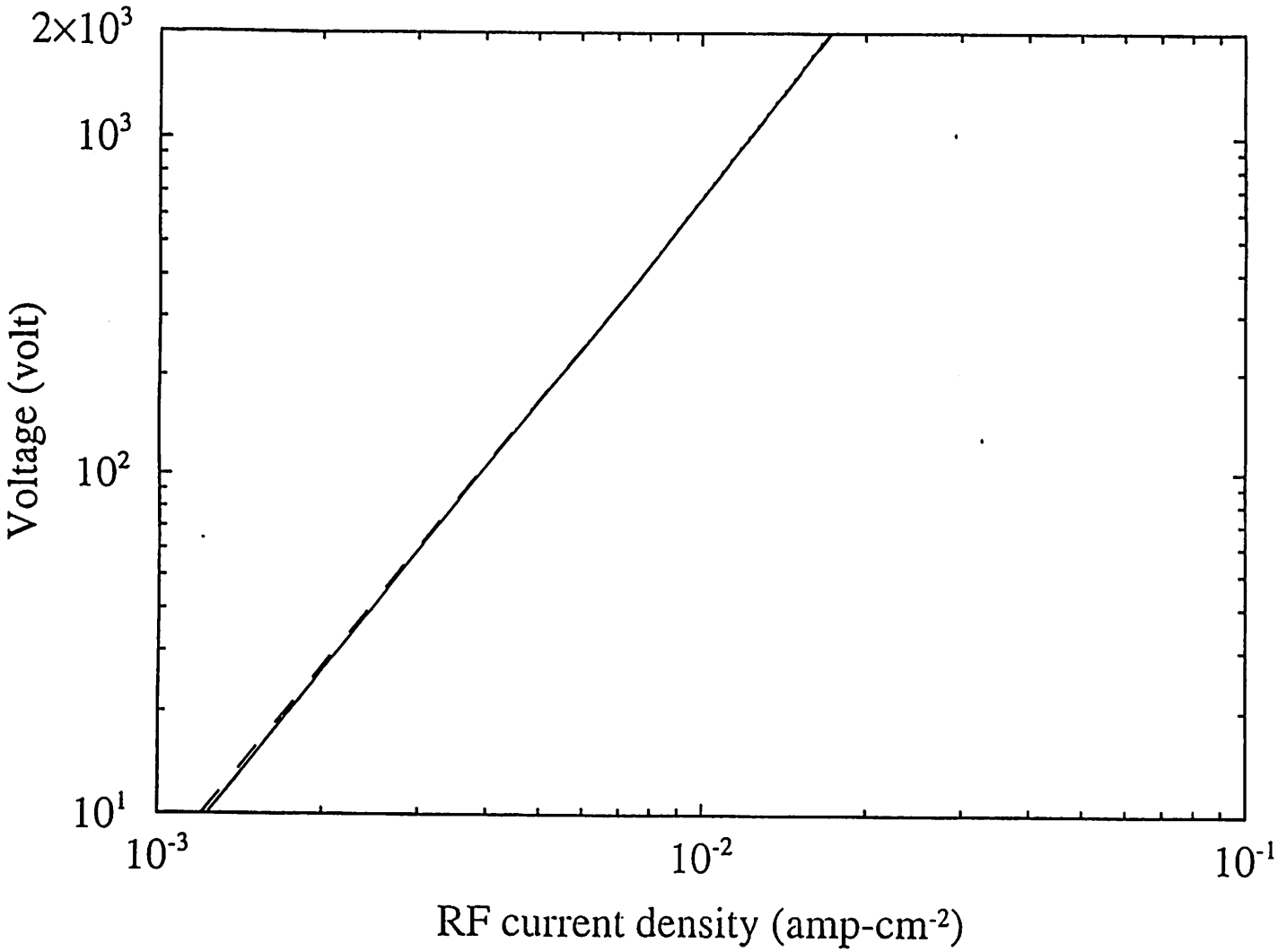

Fig. 5: Total Absorbed RF Power

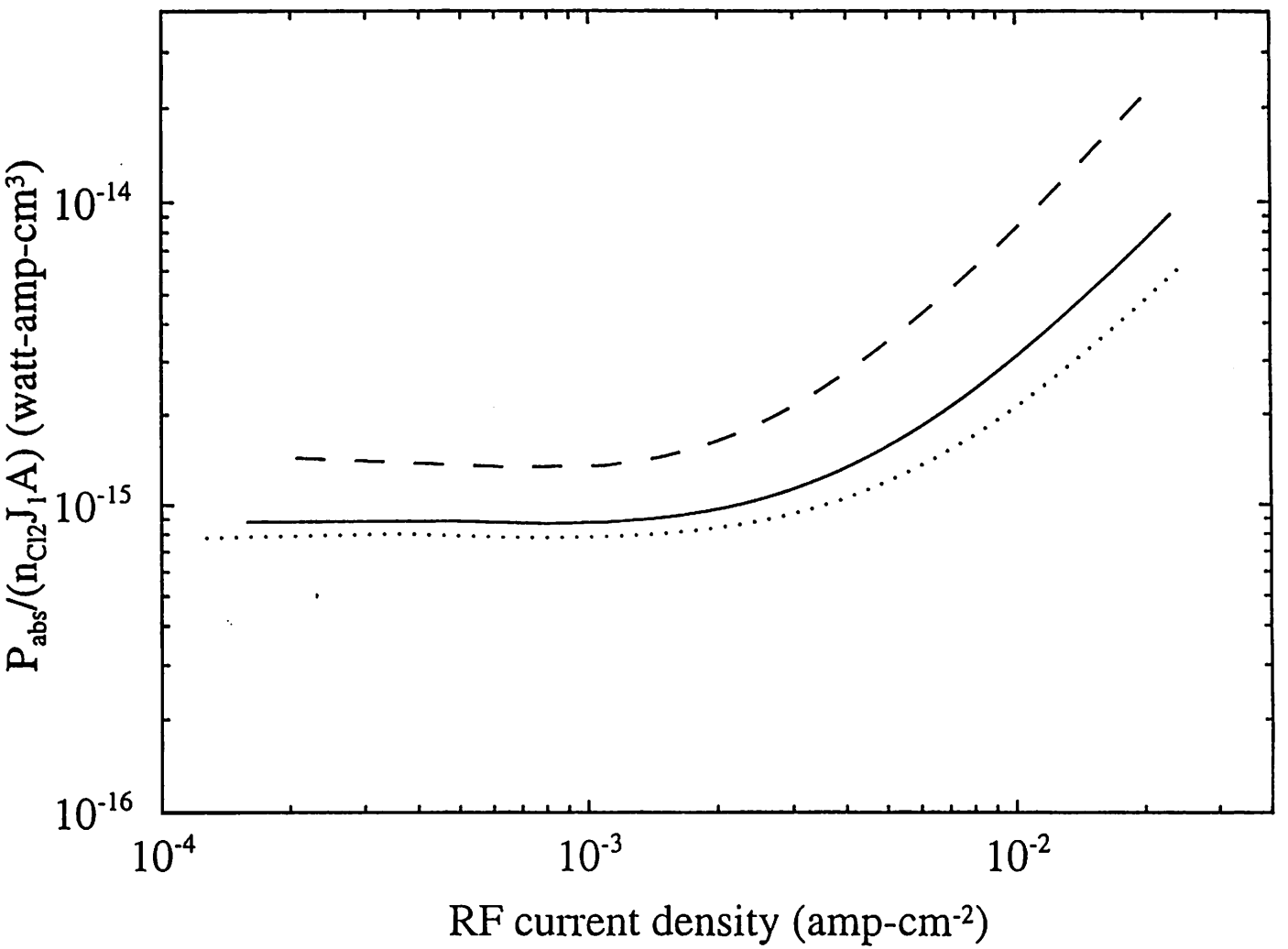

Fig. 6a: RF Current

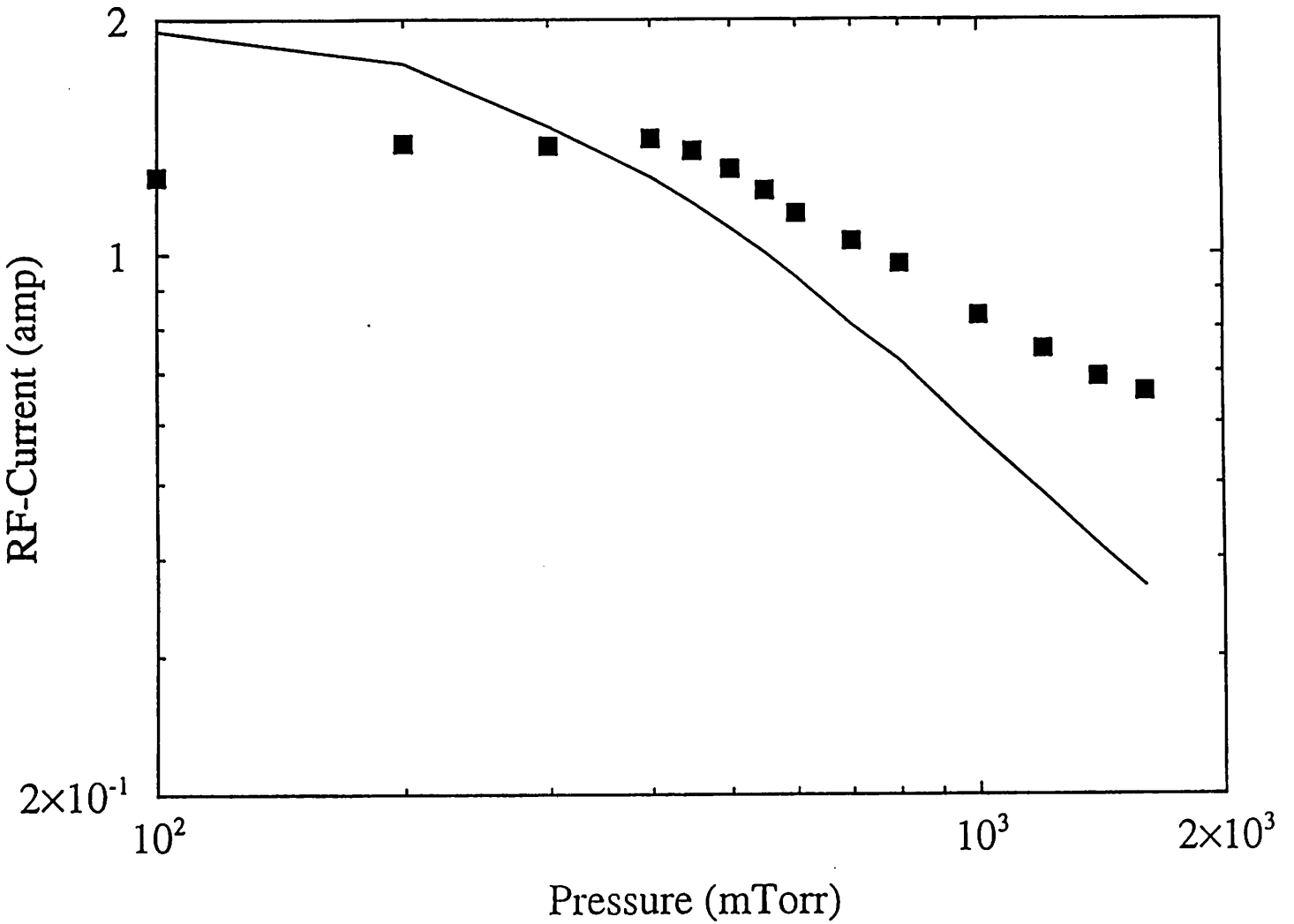

Fig. 6b: Voltage Across the Discharge

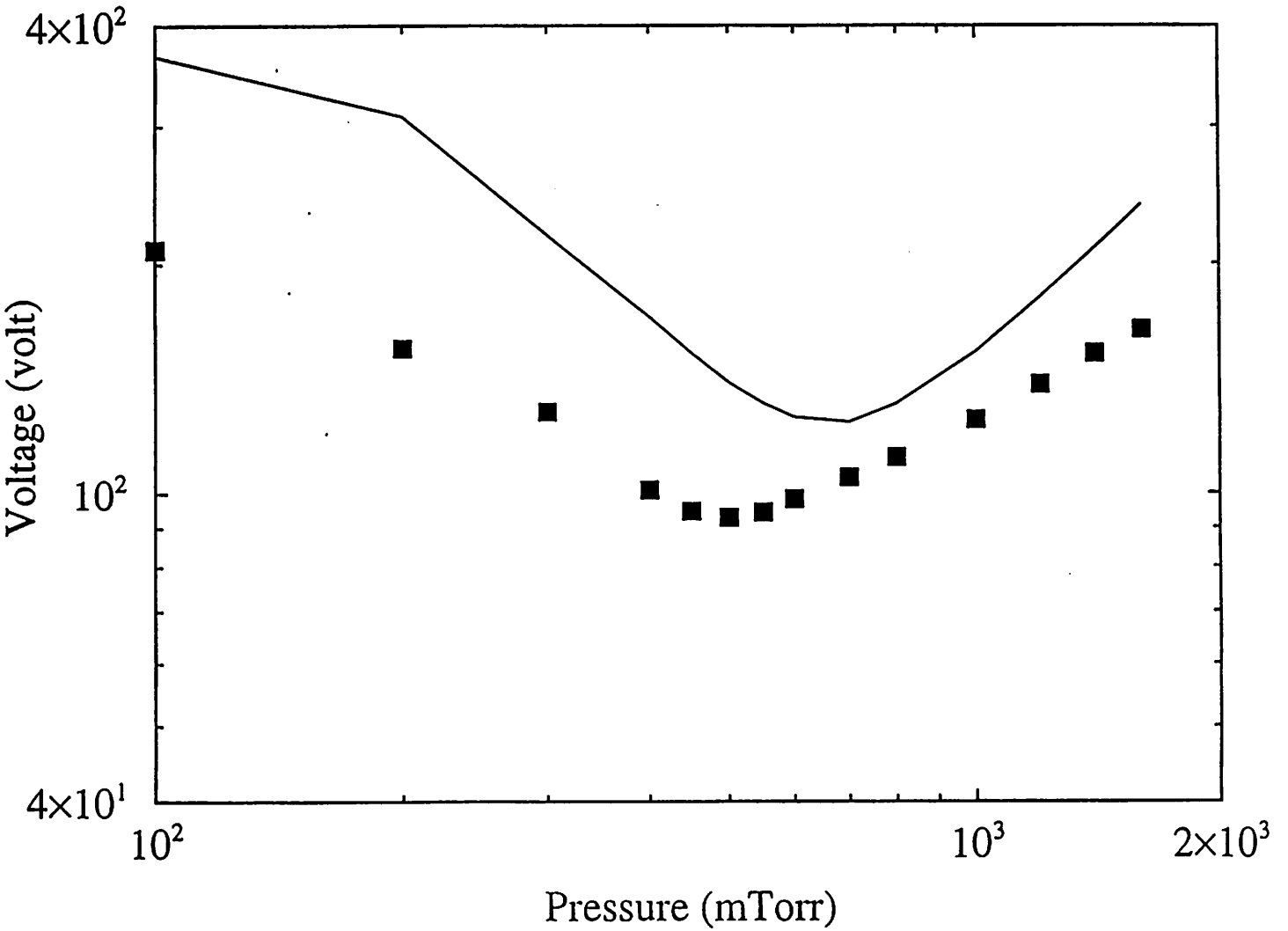

Fig. 6c: Phase Angle

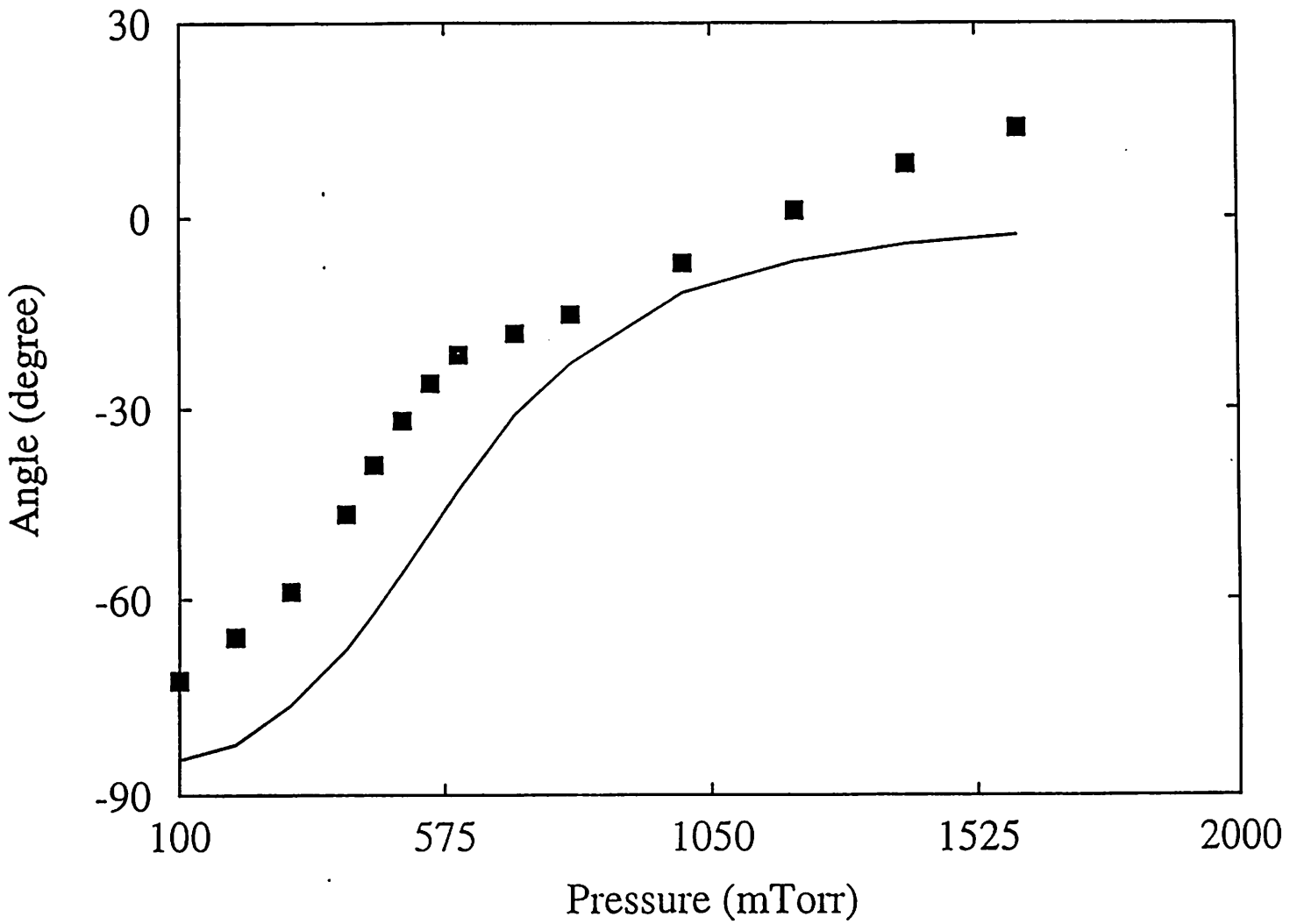

Fig. 7a: RF Current

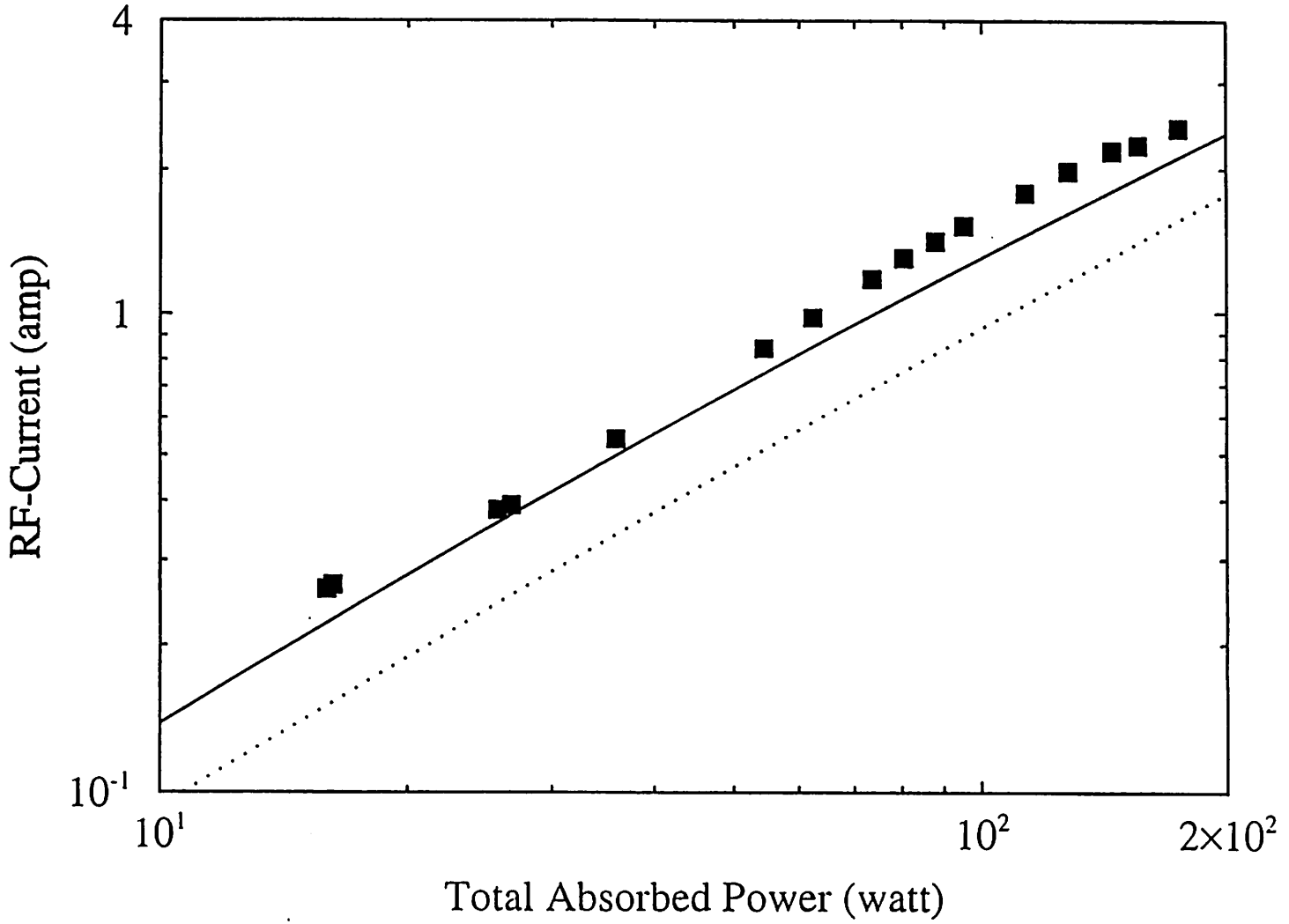

Fig. 7b: Voltage Across the Discharge

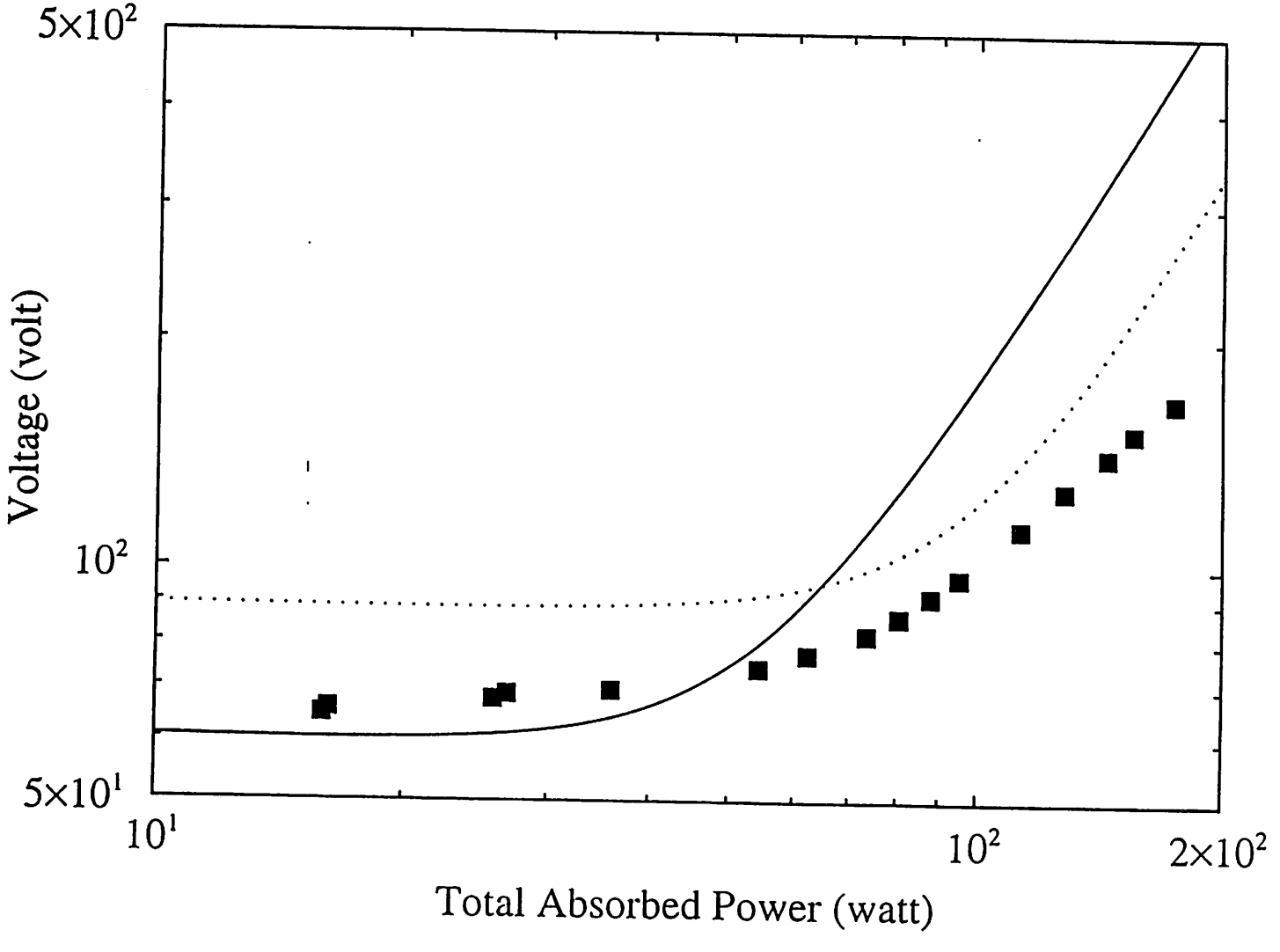

Fig. 7c: Phase Angle